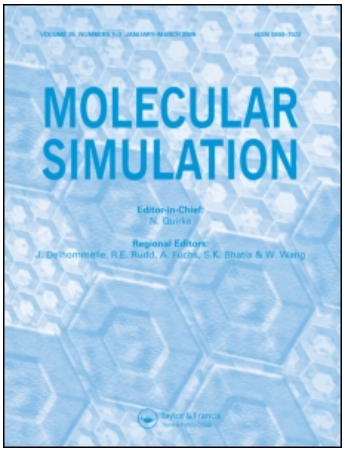

Molecular Simulation
Publication details, including instructions for authors and subscription information:
http://www.informaworld.com/smpp/title~content=t713644482

Simulation of chemical reaction equilibria by the reaction ensemble Monte Carlo method: a review†

C. Heath Turner[a]; John K. Brennan[b]; Martin Lísal[c]; William R. Smith[d]; J. Karl Johnson[e]; Keith E. Gubbins[f]
[a] Department of Chemical and Biological Engineering, University of Alabama, Tuscaloosa, USA [b] US Army Research Laboratory, Weapons and Materials Research Directorate, Maryland, USA [c] E. Hála Laboratory of Thermodynamics, Institute of Chemical Process Fundamentals, Academy of Sciences of the Czech Republic, Prague, Czech Republic [d] Faculty of Science, University of Ontario Institute of Technology, Oshawa, ON, Canada [e] Department of Chemical and Petroleum Engineering, University of Pittsburgh, Pittsburgh, USA [f] Department of Chemical and Biomolecular Engineering, North Carolina State University, Raleigh, NC, USA

To cite this Article Heath Turner, C. , Brennan, John K. , Lísal, Martin , Smith, William R. , Karl Johnson, J. and Gubbins, Keith E.(2008) 'Simulation of chemical reaction equilibria by the reaction ensemble Monte Carlo method: a review†', Molecular Simulation, 34: 2, 119 — 146
To link to this Article: DOI: 10.1080/08927020801986564
URL: http://dx.doi.org/10.1080/08927020801986564

Molecular Simulation
Vol. 34, No. 2, February 2008, 119–146

Taylor & Francis
Taylor & Francis Group

Simulation of chemical reaction equilibria by the reaction ensemble Monte Carlo method: a review†

C. Heath Turner[a]*, John K. Brennan[b], Martin Lísal[cd], William R. Smith[e], J. Karl Johnson[f] and Keith E. Gubbins[g]

[a]*Department of Chemical and Biological Engineering, University of Alabama, Tuscaloosa, USA;* [b]*US Army Research Laboratory, Weapons and Materials Research Directorate, Maryland, USA;* [c]*E. Hála Laboratory of Thermodynamics, Institute of Chemical Process Fundamentals, Academy of Sciences of the Czech Republic, Prague, Czech Republic;* [d]*Department of Physics, Faculty of Science, J.E. Purkinje University, Czech Republic;* [e]*Faculty of Science, University of Ontario Institute of Technology, Oshawa, ON, Canada;* [f]*Department of Chemical and Petroleum Engineering, University of Pittsburgh, Pittsburgh USA;* [g]*Department of Chemical and Biomolecular Engineering, North Carolina State University, Raleigh, NC, USA*

(Received 14 December 2007; final version received 9 February 2008)

Understanding and predicting the equilibrium behaviour of chemically reacting systems in highly non-ideal environments is critical to many fields of science and technology, including solvation, nanoporous materials, catalyst design, combustion and propulsion science, shock physics and many more. A method with recent success in predicting the equilibrium behaviour of reactions under non-ideal conditions is the reaction ensemble Monte Carlo method (RxMC). RxMC has been applied to reactions confined in porous solids or near solid surfaces, reactions at high temperature and/or high pressure, reactions in solution and at phase interfaces. The only required information is a description of the intermolecular forces among the system molecules and standard free-energy data for the reacting components. Extensions of the original method include its combination with algorithms for systems involving phase equilibria, constant-enthalpy and constant-internal energy adiabatic conditions, a method to include reaction kinetics, a method to study the dynamics of reacting systems, and a mesoscale method to simulate long-chain molecule phase separation. This manuscript surveys the various applications and adaptations of the RxMC method to date. Additionally, the relationship between the RxMC method and other techniques that simulate chemical reaction behaviour is given, along with insight into some technical nuances not found in the pioneering papers.

Keywords: Monte Carlo; reaction; equilibria; simulation

1. Introduction

The behaviour of chemical reactions in highly non-ideal environments spans a wide range of scientific interest, including catalyst development, nanoporous material manufacturing, supercritical fluid separation, propulsion and combustion science, shock and planetary physics, novel energy storage devices and more. The thermodynamic driving forces for chemical reactions arise from differences in the isolated molecule (ideal-gas) energetic properties of the constituent reactant and product species. In non-ideal systems, these forces are modulated by the physical forces arising from the intermolecular forces experienced by the reacting components, including interactions among the reacting compounds themselves, molecular confinement, and solvation of a surrounding fluid. A fundamental understanding of the relevant physical forces is critical for optimising processes and applications involving chemical reactions. For example, in the design of heterogeneous carbon supports (which are often highly porous materials) molecular-level confinement strongly affects the adsorbed phase, which in turn influences the reaction equilibria (and the kinetics).

Accurately measuring reaction equilibria for some systems can be extremely challenging. In particular, measurements can be hindered by the length scale. For example, measuring the concentrations of a fluid mixture confined in a nanoporous material is difficult, if not impossible. Moreover, extreme conditions such as high pressure or high temperature can require specialised instrumentation (e.g. a diamond anvil cell), limiting the types of materials and conditions that can be studied. While not all experimental measurements of reaction equilibria are difficult, future progress in understanding phenomena at the nanoscale will be a result of combined experimental and computational approaches.

Laboratory challenges have necessitated the development of theoretical predictive capabilities to complement

†Bill Smith's co-authors congratulate him on his 65th birthday.

*Corresponding author. Email: hturner@eng.ua.edu

ISSN 0892-7022 print/ISSN 1029-0435 online

DOI: 10.1080/08927020801986564
http://www.informaworld.com

the experimental analyses. To date, the most reliable theoretical treatments for predicting reaction equilibria apply statistical mechanical approaches such as variational perturbation theory (e.g. [1]) or integral equation theory (e.g. [2–8]). Ultimately, these approaches can be used to predict reaction equilibria by minimising the system Gibbs free-energy, under the constraints of conservation of the total number of atoms of each element constituting the chemically reacting species [9]. However, approximations must often be made within the theoretical models to keep the calculations tractable. These types of approximations can add uncertainty to the predictive capabilities of the methods. Traditional methods for computing reaction and phase equilibria rely upon macroscopic-level thermodynamic descriptions, such as equations of state. However, molecular simulations can provide unique insight into atomic-level phenomena, which thermodynamic models cannot.

In addition to the reaction ensemble Monte Carlo (RxMC) approach reviewed here, there has been significant development of other molecular-level and atomistic computational approaches that can also provide information about chemical reaction equilibria. These can be grouped into two general categories: *ab initio* methods and force field methods [10]. The most fundamental approach to modelling chemical reactivity is with electronic structure calculations, which are based on the principles of quantum mechanics. The electronic degrees of freedom are directly included in the calculations, which allows an accurate treatment of bond distortion, bond breaking, and bond formation energetics. In general, these calculations scale poorly, so for large systems or systems that include environmental effects (like solvation), a multi-scale hybrid treatment is often used. This is the route often taken when simulating reactions involving bulky biological fragments, where the active reaction centre is treated with quantum mechanics and the rest of the molecule is simulated using a molecular mechanics approach.

In this quantum mechanics/molecular mechanics (QM/MM) approach, the simulation cell is divided into sub-domains, based on the 'chemical significance' of each domain. Once these regions are identified, various levels of chemical detail (or level of theory) are included in the calculation. The general philosophy is to apply the minimum amount of detail (or computational effort) to each region needed to capture the emergent chemical physics of each region. For instance, domains of the simulation cell that experience significant forces or bond distortion may require a quantum mechanical treatment of the energetics, whereas other regions of the system may be adequately modelled with simple two-body empirical potentials.

Semi-empirical methods can also be used to model chemical reactivity. However, these are not true *ab initio* methods, since they are parameterised to match experimental data or data from some other high-level calculation. In retrospect, these methods give accurate results for certain systems, and the time scales and length scales accessible in these simulations are much greater than true *ab initio* approaches.

In the second general category of computational methods for simulating reaction equilibria, the strategy is to use an analytical reactive potential to describe the bond breaking and bond formation events that occur during the simulation of a chemically reactive system. The quality of the results depends heavily upon the accuracy of the potential. The reactive potential can be developed by parameterising detailed experimental data about the reaction energetics or by performing a comprehensive set of electronic structure calculations of the relevant chemical events. Once a reactive potential is made available, classical molecular dynamics (MD) simulations of the system can be performed, yielding important information about the reaction dynamics, and with long simulation times, provide estimates of the equilibrium composition.

This route has been implemented in many simulation studies and is able to provide detailed information about the system reactivity. While we do not intend to discuss these approaches in detail here, there are a few reactive potentials that have become popular. For instance, the reactive empirical bond-order (REBO) potential of Brenner adequately describes bonding in carbonaceous systems, and it has been extended (i.e. re-parameterised) in more recent studies to account for metal–metal and metal–carbon interactions [11,12]. The REBO potential has also been modified to model the reactivity of condensed-phase hydrocarbon systems [13], and this modified potential is called the adaptive intermolecular REBO or adaptive intermolecular REBO (AIREBO) potential [14–17]. Another popular reactive potential is the ReaxFF [18], which was intended to improve the REBO potential energy curves for bond-breaking events. This potential has been applied to many systems, but the parameterisation can be tedious, since atom pairs, valence angles, torsions, and conjugation must be included, as well as the total potential energy. In practice, the ReaxFF is computationally demanding, but multi-scale hybrid approaches have been used to extend this potential to systems of $\sim 10^9$ atoms on large multi-processor machines [19–21]. The main drawbacks of these empirical force field methods are: (1) they have been developed for a relatively limited number of materials; and (2) they are sensitive to the parameterisation, such that predictions of reactivity at only slightly different conditions may not be reliable. A more thorough discussion of the many *ab initio* and force field approaches used to describe chemical reactivity can be found in Ref. [10].

While both *ab initio* and force field approaches have significant drawbacks, nonetheless, they are effective routes for following the short-time transient behaviour

of a reactive system. However, when the focus shifts to prediction of equilibrium behaviour, the direct simulation of bond breaking and bond formation is no longer necessary because the equilibrium conversion of a chemical reaction results from the free energy difference between the reactants and the products. This implies that the path from reactants to products is irrelevant, with respect to the final value of the equilibrium conversion. The RxMC simulation method uses Monte Carlo (MC) sampling to directly simulate pre-defined forward and reverse reaction events in a simulation, yielding the equilibrium composition of the reacting mixture. In these simulations, completed forward and reverse reaction events are sampled, so that the energetics of bond breaking and bond formation are unnecessary. Furthermore, since the activation barriers for the reactions are eliminated in these simulations, kinetic limitations are circumvented and equilibrium can be established very rapidly under various conditions. The RxMC approach can be performed in any number of basic ensembles, and its implementation is similar to a traditional grand canonical MC (GCMC) simulation for a multicomponent mixture, since it involves molecular insertions and deletions, and changes of particle identities during the simulation.

In a non-ideal environment (e.g. a condensed phase, a porous material or a supercritical solvent), the RxMC approach can be thought of as predicting the shift in chemical equilibrium conversion which deviates from the ideal-gas phase reaction equilibrium involving the same reactions and constituents. RxMC simulations provide equilibrium concentrations for each species, and (depending on the thermodynamic variables specified for the system) relevant thermodynamic properties such as the density, pressure, and energy, in addition to the fluid structure. Multiple reactions and multiple phases can be simulated simultaneously. Due to its thermodynamic origin, the method does not require a reactive potential that mimics bond breaking or forming. Furthermore, it is not limited by the rate of the reaction or by the height of the activation energy barrier. It requires only ideal-gas free energy information for the specified set of reacting species and a description of the relevant intermolecular forces.

In the RxMC method, the reaction set that is used in the simulation must be specified. This reaction set is arbitrary, apart from the requirement that it provide a proper description of the underlying chemical stoichiometry (see [9], Chapter 2). The computational efficiency of the RxMC method may be improved by investigating alternative reaction sets at the equilibration stage of the simulation. RxMC predicts the equilibrium compositions of only the specified reaction species and will not create new species that have not been explicitly included in the reaction set. Although we will show later that RxMC can provide reaction rate information for some systems [22], no direct kinetic or rate information can in general be gained from an RxMC simulation.

The RxMC method can encounter some technical hurdles, which are similar to those arising for other MC simulations. To mimic chemical reactions in an RxMC simulation, reactant molecules are removed from the simulation cell while product molecules are simultaneously inserted into the simulation cell. For some systems, e.g. high density and low temperature conditions, the insertion and deletion of molecules can be energetically unfavourable, making the RxMC method extremely inefficient in such cases. However, advances have been made to help overcome this computational challenge and extend the range of the application of the method [23,24] (reviews of these methods are given in Section 4.5 and 4.6, respectively).

In addition to specifying the reaction set that is occurring, two other pieces of information are needed to perform an RxMC simulation. First, details of the ideal-gas phase reaction are required, i.e. the intramolecular contributions for the reactants and products in the ideal-gas state, which include vibrational, rotational and electronic contributions. Either thermochemical data tables or quantum mechanics calculations can provide the necessary information to determine these intramolecular contributions. The second piece of information required to perform an RxMC simulation is a set of intermolecular potentials describing the interactions between reactants, products and where appropriate, the non-ideal environment, e.g. a pore wall.

The RxMC method was independently published by two different groups in 1994 [25,26]. A method similar to RxMC was also developed independently during the same time frame by Shaw termed the '$N_{\text{atoms}}PT$ ensemble' [27–30]. Shaw's method is similar to RxMC in that it does not require the specification of chemical potentials or chemical potential differences. However, when simulating reactions in which the number of moles is not conserved, the $N_{\text{atoms}}PT$ ensemble requires implementation of the concept of a *null* particle. The relationship between RxMC and the $N_{\text{atoms}}PT$ ensemble as well as other methods developed for the statistical mechanics modelling of chemical reactions can be found in a review by Johnson [31]. The methods of Johnson et al. and Smith and Tříska are essentially the same with only slight differences with regards to how the ideal-gas phase reaction behaviour is specified in the acceptance criteria. The formalism found in the work of Johnson et al. preserves the intramolecular partition functions of the reactants and products in the acceptance criteria for the forward and reverse reaction steps. Smith and Tříska group the individual partition functions together and then use the overall free energy of reaction, which is typically more readily accessible, within the acceptance criteria. In these original developments, Johnson et al. applied the RxMC method to model reaction and phase equilibria in the

context of an association reaction, while Smith and Tříska applied the RxMC method to simulate a general multi-phase multi-species reacting system.

A variety of nomenclature and shorthand notation has been used for the RxMC method, all of which refer to the same method. Johnson and co-workers used the term 'reactive canonical Monte Carlo' and the notation 'RCMC', while Smith and Tříska used the term 'reaction ensemble' without any shorthand notation. Other workers have used the terms 'reactive Monte Carlo' and 'RxMC' and the notations 'REMC' and 'RxMC'. In this review, we use the nomenclature 'RxMC' and the shorthand notation 'RxMC'.

The overall objective of the manuscript is to provide a review of the applications and extensions of the RxMC method that have been published to date. We hope the manuscript provides insight into the RxMC method that the reader cannot glean from the pioneering papers. We also hope to further clarify the relationship between RxMC and other computational methods that simulate chemical reaction equilibria. Applications of the RxMC simulation method to date include numerous bulk phase reaction studies [32–36], combined reaction and phase equilibria [25,37,38], reactions confined in porous materials [32,39–46], reactions in plasmas [47,48], reactions in supercritical fluid solvents [49], reactions under shock [50–53], and still others [54–57]. Extensions of the method to date include a constant total internal energy or constant total enthalpy method [58], a method to study reaction kinetics [22], methods to study the dynamics of reacting systems [59,60] and a method to simulate macro- and micro-phase separation at the mesoscale [61]. Before reviewing these applications and developments, we provide a detailed description of the method in its various forms.

2. Derivation and detailed description of the RxMC method

We provide a derivation of the RxMC method in the case of a single chemical reaction occurring in one phase at specified temperature T and system volume V. We will then generalise the derivation to allow for specified T and pressure P systems, and/or multiple reactions and multi-phase systems.

A single chemical reaction in one-phase at specified (T, V) can be expressed as

$$\sum_{i=1}^{s} \nu_i S_i = 0, \tag{1}$$

and simulated by considering 'reaction steps' (consisting of the simultaneous insertion and deletion of molecules in the system according to the stoichiometry of the reaction with appropriate acceptance probabilities) that guarantee that the reaction equilibrium criterion for the chemical reaction given in Equation (1)

$$\sum_{i=1}^{s} \nu_i \mu_i = 0, \tag{2}$$

is established [9]. In Equations (1) and (2), ν_i is the stoichiometric number of species i, S_i denotes the chemical symbol of species i, μ_i is its chemical potential and s is the total number of chemical species. Changes in the number of particles ($N_i \geq 0$) due to the reaction steps satisfy the law of conservation of mass for the system, which may be expressed as

$$N_i = N_i^0 + \nu_i \xi \quad (i = 1, 2, \ldots, s), \tag{3}$$

where ξ is the extent of reaction and N_i^0 is the number of molecules of species i in the state prior to a reaction step. In the RxMC approach, ξ is an integer and the efficiency of the method typically requires using a value of ξ equal to $+1$ or -1.

Next, we consider transitions from an initial state k (prior to a reaction step) to a final state l (after the reaction step) in which the reaction proceeds either 'forward' ($\xi = +1$) or 'reverse' ($\xi = -1$) with the aim of determining transition probabilities for the forward and reverse reaction moves. In the following, we assume that the reaction events are attempted in the forward and the reverse directions with equal probability. To derive the transition probabilities for these events, we start with the grand canonical partition function for a mixture of s components [62].

$$\Xi = \sum_{N_1=0}^{\infty} \cdots \sum_{N_s=0}^{\infty} \int \cdots \int \exp\left[\beta \sum_{i=1}^{s} N_i \mu_i - \sum_{i=1}^{s} \ln(N_i!) + \sum_{i=1}^{s} N_i \ln \frac{V q_i}{\Lambda_i^3} - \beta U\right] \mathrm{d}s^{N_1} \mathrm{d}\omega^{N_1} \ldots \mathrm{d}s^{N_s} \mathrm{d}\omega^{N_s}, \tag{4}$$

where $\beta = 1/(k_B T)$, k_B is the Boltzmann constant, $q_i = q_{i,r} q_{i,v} q_{i,e} q_{i,n}$ is the internal contributions (rotational, vibrational, electronic, nuclear) to the partition function for isolated molecule i, Λ_i is its de Broglie thermal wavelength, U is the configurational energy of the mixture, $s = r/V^{1/3}$ is a set of scaled coordinates, and ω is a set of orientations. The q_i term is related to the molar standard chemical potential μ_i^0 [9,63] via

$$\frac{\mu_i^0}{RT} = -\ln\left(\frac{q_i}{\beta P^0 \Lambda_i^3}\right), \tag{5}$$

where R is the universal gas constant and P^0 is the standard-state pressure (typically taken to be one bar). Accurate and readily available values for μ_i^0 are contained in thermochemical compilations such as the Thermodynamics Research Center (TRC) [64] or NIST-JANAF tables [65]. The probability that a system is in state k is then

$$P_k = \frac{1}{\Xi}\exp\left[\beta\sum_{i=1}^{s} N_i\mu_i - \sum_{i=1}^{s}\ln(N_i!) + \sum_{i=1}^{s} N_i \ln\frac{Vq_i}{\Lambda_i^3} - \beta U_k\right], \tag{6}$$

where U_k is the configurational energy of state k. If the reaction in Equation (1) proceeds in the forward direction ($\xi = +1$) from state k to state l, then N_i changes according to Equation (3) and the probability of observing that state is

$$P_l = \frac{1}{\Xi}\exp\left\{\beta\sum_{i=1}^{s}(N_i+\nu_i)\mu_i - \sum_{i=1}^{s}\ln[(N_i+\nu_i)!] + \sum_{i=1}^{s}(N_i+\nu_i)\ln\frac{Vq_i}{\Lambda_i^3} - \beta U_l\right\}, \tag{7}$$

where U_l is the configurational energy of state l. The transition probability for the reaction in the forward direction, $P_{k\to l}^{+1}$, is then given as the ratio of P_l/P_k, i.e.

$$P_{k\to l}^{+1} = \min\left\{1, V^{\bar\nu}\prod_{i=1}^{s}\left(\frac{q_i}{\Lambda_i^3}\right)^{\nu_i}\prod_{i=1}^{s}\left[\frac{(N_i^0)!}{(N_i^0+\nu_i)!}\right] \exp(-\beta\Delta U_{kl})\right\}, \tag{8}$$

where $\bar\nu = \sum_{i=1}^{s}\nu_i$ is the net change in the total number of molecules for the reaction given in Equation (1) and $\Delta U_{kl} = U_l - U_k$. Note that the chemical potentials have cancelled out of Equation (8) by application of the reaction equilibrium criterion, Equation (2). Analogously, we can derive the transition probability for the reaction in the reverse direction ($\xi = -1$), $P_{k\to l}^{-1}$, and in doing so we get

$$P_{k\to l}^{-1} = \min\left\{1, V^{-\bar\nu}\prod_{i=1}^{s}\left(\frac{q_i}{\Lambda_i^3}\right)^{-\nu_i}\prod_{i=1}^{s}\left[\frac{(N_i^0)!}{(N_i^0-\nu_i)!}\right] \exp(-\beta\Delta U_{kl})\right\} \tag{9}$$

By introducing the ideal-gas equilibrium constant

$$K = \exp\left(-\frac{\sum_{i=1}^{s}\nu_i\mu_i^0}{RT}\right) \tag{10}$$

Equations (8) and (9) can be written in a more compact form as

$$P_{kl}^{\xi} = \min\left\{1, (\beta P^0 V)^{\bar\nu\xi} K^{\xi}\prod_{i=1}^{s}\left[\frac{(N_i^0)!}{(N_i^0+\nu_i\xi)!}\right]\exp(-\beta\Delta U_{kl})\right\}. \tag{11}$$

To simulate a chemical reaction at specified (T, P), rather than at specified (T, V), we simply incorporate trial volume changes $V_k \to V_l$ in addition to the particle displacements/reorientations and reaction moves. The trial volume changes are governed by [66]

$$P_{kl}^{V} = \min\left\{1, \exp\left[-\beta\Delta U_{kl} - \beta P(V_l - V_k) + N\ln\frac{V_l}{V_k}\right]\right\} \tag{12a}$$

or by

$$P_{kl}^{V} = \min\left\{1, \exp\left[-\beta\Delta U_{kl} - \beta P(V_l - V_k) + (N+1)\ln\frac{V_l}{V_k}\right]\right\}, \tag{12b}$$

where $N = \sum_{i=1}^{s} N_i$ is the total number of molecules in the system. Equations (12a) and (12b) are valid when performing random walks in V and $\ln V$, respectively.

The RxMC approach outlined above for a single chemical reaction can be straightforwardly generalised to any linearly independent set of R_t chemical reactions, given by

$$\sum_{i=1}^{s_j}\nu_{ji}S_i = 0 \quad (j = 1, 2, \ldots, R_t), \tag{13}$$

where ν_{ji} is the stoichiometric number of species i in reaction j and s_j is the number of species in reaction j. In the case of multiple chemical reactions, Equations (2) and (3) then read as

$$\sum_{i=1}^{s_j}\nu_{ji}\mu_i = 0 \quad (j = 1, 2, \ldots, R_t) \tag{14}$$

$$N_i = N_i^0 + \sum_{j=1}^{R_t}\nu_{ji}\xi_j \qquad (i = 1, 2, \ldots, s; j = 1, 2, \ldots, R_t), \tag{15}$$

and the transition probability for an individual reaction step ξ_j is then

$$P_{kl}^{\xi_j} = \min\left\{1, (\beta P^0 V)^{\bar\nu_j\xi_j} K_j^{\xi_j}\prod_{i=1}^{s_j}\left[\frac{(N_i^0)!}{(N_i^0+\nu_{ji}\xi_j)!}\right]\exp(-\beta\Delta U_{kl})\right\}, \tag{16}$$

where $\bar{\nu}_j = \sum_{i=1}^{s_j} \nu_{ji}$ is the net change in the total number of molecules for reaction j and

$$K_j = \exp\left(-\frac{\sum_{i=1}^{s_j} \nu_{ji}\mu_i^0}{RT}\right). \tag{17}$$

To summarise, the RxMC method (for a single-phase system) consists of a combination of the following types of MC steps:

(1) Particle displacements/reorientations;
(2) Reactions, consisting of the following:
    (a) Randomly select a reaction if $R_t > 1$;
    (b) Randomly select the reaction direction, forward or reverse;
    (c) Randomly select a set of reactant and product molecules in the system according to the stoichiometry of the selected reaction;
    (d) Attempt the reaction move by evaluating the acceptance probability associated with performing changes of particle identities, together with particle insertions and deletions, if the total number of molecules changes during the selected reaction;
(3) Volume changes in the case of constant-P simulations.

The convergence rate of the method is influenced by the relative ratios of the three different types of steps, with the optimal choice depending on the system properties and the state point simulated. The relative frequency of steps 1, 2 and 3 should be chosen similarly to steps performed in conventional GCMC and isothermal-isobaric MC simulations, i.e. $\bar{N} : 1 : (1 \div 10)\bar{N}$, where $\bar{N}$ is approximately the anticipated total number of molecules. To increase the sampling efficiency, it is convenient (e.g. in the case of multiple reactions at extreme thermodynamic conditions) not to select particular reactions randomly but in such a way as to ensure that the number of *accepted* reactions is equivalent for each reaction type; for details, see [56].

The RxMC method can be combined with the Gibbs ensemble Monte Carlo (GEMC) technique [67,68] to simulate combined reaction and phase equilibria (typically vapour–liquid). Note that phase equilibria can be regarded as a special case of chemical reaction, according to

$$1 \cdot S_i^a - 1 \cdot S_i^b = 0 \quad (i = 1, 2, \ldots, s), \tag{18}$$

where S_i^a and S_i^b denote the chemical symbol of species i in phase a and in phase b, respectively. The relevant phase equilibrium conditions then follow from Equation (2) and read as

$$\mu_i^a = \mu_i^b \quad (i = 1, 2, \ldots, s) \tag{19}$$

As in the GEMC approach, each phase is modelled by a separate box. In addition to particle displacements/reorientations, reaction and volume-change steps, inter-phase particle transfers are incorporated into the RxMC method to ensure equality of chemical potentials between phases. Implementation of the inter-phase particle transfers depends on the algorithm used [69]. Therefore, in the following, we provide details of all three possible particle-transfer algorithms for completeness.

The first algorithm [68,69] involves randomly choosing species i and donor box a, and subsequently transferring that species to a random position in recipient box b. The corresponding transition probability is given by

$$P_{kl}^{\mathrm{t}} = \min\left\{1, \frac{N_i^a V^b}{(N_i^b + 1)V^a} \exp\left(-\beta\Delta U_{kl}^a - \beta\Delta U_{kl}^b\right)\right\}. \tag{20}$$

The second algorithm [69] involves randomly choosing the particular particle that is to be transferred from one of the N particles of the total system regardless of which box it is in or its species type. The transition probability in this case is given by

$$P_{kl}^{\mathrm{t}} = \min\left\{1, \frac{V^b}{V^a} \exp\left(-\beta\Delta U_{kl}^a - \beta\Delta U_{kl}^b\right)\right\}. \tag{21}$$

The third algorithm [69] involves choosing the donor box a and recipient box b at random, then randomly choosing the particle that is to be transferred from the donor box regardless of its type, and subsequently transferring it to a random position in the recipient box. The corresponding transition probability is given by

$$P_{kl}^{\mathrm{t}} = \min\left\{1, \frac{N^a V^b}{(N^b + 1)V^a} \exp\left(-\beta\Delta U_{kl}^a - \beta\Delta U_{kl}^b\right)\right\}. \tag{22}$$

The RxMC simulation strategy in the case of combined reaction and phase equilibria depends on the complexity of the reactive systems. The particle displacement/reorientation steps are carried out in each phase. The volume change steps are also performed for each box in the case of constant-pressure simulations (unless it violates the Gibbs phase rule). It should be noted that for some multiphase reactive systems, such as vapour–liquid equilibrium, with a dimerisation reaction $2\mathrm{A} \leftrightarrow \mathrm{B}$, the pressure cannot be specified in advance (simultaneous specification of T and P will result in a single-phase system unless the conditions are exactly on the saturation curve). Rather, the equality of pressure in the vapour and liquid phase is achieved by correlated

volume changes as in the GEMC simulation of pure substances, which are governed by [67]

$$P_{kl}^{V} = \min\left\{1, \exp\left[-\beta\Delta U_{kl}^{a} - \beta\Delta U_{kl}^{b} + N^{a}\ln\left(\frac{V_k^a + \Delta V}{V_k^a}\right) + N^{b}\ln\left(\frac{V_k^b - \Delta V}{V_k^b}\right)\right]\right\}, \tag{23}$$

where ΔV is a random volume change.

For a multiphase reacting system, the chemical reaction steps may be carried out either in each phase or in one phase only (typically in the less dense phase). However, computational efficiency will be affected by that choice. When reaction steps are carried out in each phase, not all species of the reactive mixture need to be transferred between boxes since the equality of the chemical potentials between phases for the other species is achieved by the reaction steps carried out for each box. In general, the total number of chemical and phase equilibrium reactions is given by $2s - \text{rank}(\mathbf{A})$, where $\mathbf{A}$ denotes the matrix formed by the molecular formulae of the species ([9], Chapter 2). To maximise efficiency, the choice of the species to be transferred between the boxes should be based upon their molecular complexity. It is desirable to transfer the smaller or simpler molecules and to avoid transferring the larger, polyatomic molecules between the boxes. The inter-phase particle transfers are then performed using the first particle-transfer algorithm, Equation (20). When reaction steps are carried out in one phase only, one of the three algorithms for particle transfers may be employed and the choice of the particle-transfer algorithm affects the efficiency in the RxMC sampling (but not the final results). The relative frequency of the particle displacements/reorientations, reaction and volume change steps are chosen similar to the one-phase RxMC case, and likewise the frequency of the particle-transfer steps should be similar to that for the reaction steps.

To conclude this section, we consider an illustrative example of a reactive distillation process with the reaction type $\text{A} + \text{B} \leftrightarrow \text{C}$, and provide additional implementation details for the RxMC method (such a system was considered by Lísal et al. [38]). In the reactive distillation process, the product C is synthesised from the reactants A and B in a liquid phase and the reaction product C is separated by distillation. The reactive distillation process thus corresponds to a vapour–liquid equilibrium system at fixed (T, P) with the reaction $\text{A} + \text{B} \leftrightarrow \text{C}$ carried out in the liquid phase [70]. The phase and reaction equilibrium of the $\text{A} + \text{B} \leftrightarrow \text{C}$ system at fixed (T, P) requires establishing equilibrium for the following chemical reactions:

$$\text{A}(v) \leftrightarrow \text{A}(l) \tag{24a}$$

$$\text{B}(v) \leftrightarrow \text{B}(l) \tag{24b}$$

$$\text{C}(v) \leftrightarrow \text{C}(l) \tag{24c}$$

$$\text{A} + \text{B} \leftrightarrow \text{C}, \tag{24d}$$

where v and l denote the vapour and liquid phases, respectively. In Equation (24d), each species may be in either phase. There are four independent stoichiometric reactions for this system, and the above form a linearly independent set. The relevant phase and reaction equilibrium conditions (*cf.* Equations (2) and (19)) are given by

$$\mu_{\text{A}}^{v} = \mu_{\text{A}}^{l} \tag{25a}$$

$$\mu_{\text{B}}^{v} = \mu_{\text{B}}^{l} \tag{25b}$$

$$\mu_{\text{C}}^{v} = \mu_{\text{C}}^{l} \tag{25c}$$

$$\mu_{\text{A}} + \mu_{\text{B}} = \mu_{\text{C}}. \tag{25d}$$

The transition probabilities for the forward ($\xi = +1$) and reverse ($\xi = -1$) reaction moves (*cf.* Equation (11)) then become:

$$P_{k\to l}^{+1} = \min\left\{1, \frac{K}{\beta P^0 V}\frac{N_{\text{A}}N_{\text{B}}}{N_{\text{C}}+1}\exp(-\beta\Delta U_{kl})\right\} \tag{26a}$$

$$P_{k\to l}^{-1} = \min\left\{1, \frac{\beta P^0 V}{K}\frac{N_{\text{C}}}{(N_{\text{A}}+1)(N_{\text{B}}+1)}\exp(-\beta\Delta U_{kl})\right\}, \tag{26b}$$

where $K = \exp\left[-(\mu_{\text{C}}^0 - \mu_{\text{A}}^0 - \mu_{\text{B}}^0)/(RT)\right]$. The reaction moves are carried out in forward and reverse directions with equal probabilities. In the forward direction, an A molecule and a B molecule (reactants) are chosen at random, and an attempt is made to simultaneously replace the A molecule by a C molecule (product) and to delete the B molecule from the system. The attempt is accepted with the probability given by Equation (26a). In the reverse direction, a C molecule (product) is chosen at random, and an attempt is made to simultaneously replace the C molecule by an A molecule (reactant) and to randomly insert a B molecule (reactant) into the box. The attempt is accepted with the probability given by Equation (26b).

In the above, we have assumed that the A and C molecules are of similar size and that the B molecules are easier to insert and delete compared to the A and C molecules. For this case, this achieves the maximum efficiency in terms of convergence of the algorithm. Note that the implementation of the reaction step is consistent with microscopic reversibility since the forward move of replacing an A molecule by a C molecule can

be immediately revisited by the reverse move of replacing a C molecule by an A molecule. Microscopic reversibility would be violated if, e.g. in the reverse move, a C molecule was replaced by a B molecule (with an A molecule inserted elsewhere in the box).

In the RxMC simulations of reactive distillation, the vapour and liquid phases are represented by two separate boxes and the required conditions of vapour–liquid and reaction equilibrium are ensured by performing a combination of four steps: particle displacements/reorientations, volume changes to maintain constant pressure, inter-phase particle transfers for the phase equilibria, and reaction steps corresponding to the reaction equilibrium. The reaction moves for the $A + B \leftrightarrow C$ reaction performed using the transition probabilities given by Equations (26a) and (26b) need be carried out only in one box for the system at hand, since Equations (24a)–(24d) form a maximal linearly independent set of chemical equations. It is usually most efficient to perform the reaction moves involving species in the less dense phase, i.e. the vapour box. The inter-phase particle transfers for A, B and C molecules are then performed using one of the three particle-transfer algorithms described above (Equations (20)–(22)). Another possible strategy, which would affect the convergence but not the final results, involves performing the reaction steps in both the vapour and liquid boxes and transferring only two species (e.g. A and B) between the boxes using the first particle-transfer algorithm, Equation (20). The phase and reaction equilibrium conditions corresponding to this case would be

$$\mu_A^v = \mu_A^l \tag{27a}$$

$$\mu_B^v = \mu_B^l \tag{27b}$$

$$\mu_A^v + \mu_B^v = \mu_C^v \tag{27c}$$

$$\mu_A^l + \mu_B^l = \mu_C^l. \tag{27d}$$

3. Applications of RxMC

The RxMC method has been applied to a wide variety of reacting systems. Below we present a review of all applications that have appeared in the literature to date, including simple bulk-phase reactions, combined chemical and phase equilibria, reactions at high pressure and high temperature, confined reactions, and reactions at interfaces.

3.1 Bulk phase reactions

The RxMC method has been applied to various idealised models as well as realistic reaction systems in bulk fluid phases. Smith and Tříska [26] tested the method on the isomerisation reaction $A \leftrightarrow B$, the dimerisation reaction $2A \leftrightarrow A_2$, the combination reaction $A + B \leftrightarrow C$, and a two-reaction system for hard sphere mixtures. They compared the RxMC simulations with results obtained using Boublík's equation of state and found excellent agreement. Smith and Tříska [26] also studied the NO formation reaction, $N_2 + O_2 \leftrightarrow 2NO$, which had been previously considered by Shaw [27]; their RxMC results were in essentially exact agreement with Shaw's results. Johnson et al. [25] tested the RxMC method on the dimerisation reaction $2A \leftrightarrow B$ with monomers A modelled as Lennard-Jones (LJ) spheres and dimers B modelled as two-centre LJ (2CLJ) diatomics. They compared the RxMC results with results obtained using the GCMC method. The agreement between the RxMC and GCMC runs was excellent. Johnson et al. [25] and Turner et al. [32] considered the NO dimerisation reaction $2NO \leftrightarrow (NO)_2$. The reactive system was modelled as a mixture of LJ and 2CLJ molecules, with the RxMC results for the bulk saturated liquid phase comparing favourably with experimental data (see Figure 1). Turner et al. [32] also studied the ammonia synthesis reaction $N_2 + 3H_2 \leftrightarrow 2NH_3$ in the compressed fluid phase, with N_2, H_2 and NH_3 modelled using all-atom potentials. They considered an initial stoichiometric mixture of N_2 and H_2 (1:3), with and without the addition of inert gases, and again the simulation results agreed quite well with experimental measurements (see Figure 2).

The predictive power of the RxMC method in the bulk phase was explored more recently by Carrero-Mantilla and Llano-Restrepo [33,34]. In [33], they studied the vapour-phase reaction equilibrium for the hydrogenation of benzene to cyclohexane reaction: $C_6H_6 + 3H_2 \leftrightarrow C_6H_{12}$. Hydrogen was modelled using

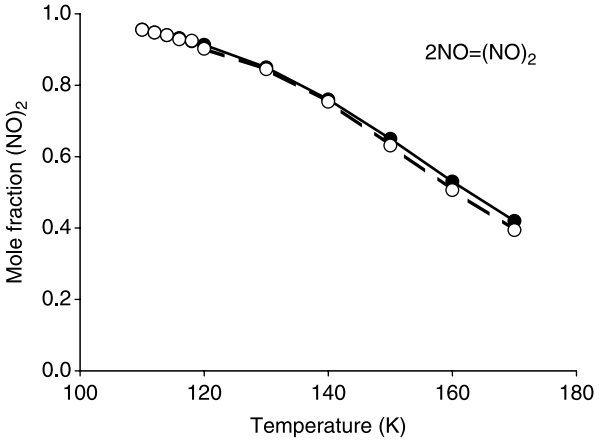

Figure 1. Mole fraction of $(NO)_2$ dimers for the bulk phase saturated liquid. The solid points and line represent experimental data. The open points and dashed line correspond to RxMC simulations. Reprinted with permission from [32]. Copyright 2001, American Institute of Physics.

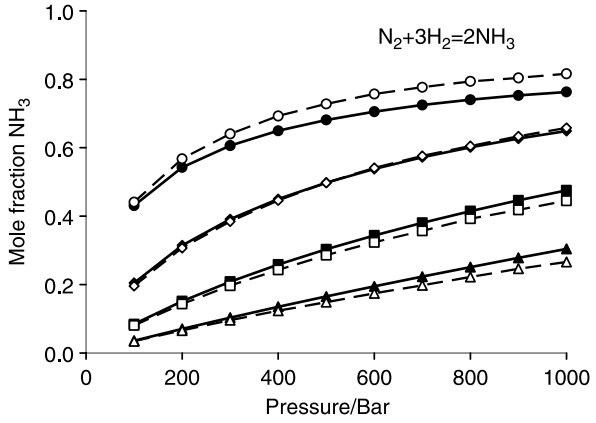

Figure 2. Mole fraction of ammonia for the bulk phase reaction of N_2 and H_2 in a 1:3 mixture, with the addition of inert gases (2.5 mol% Ar; 7.5 mol% CH_4). The solid points and solid lines represent a fit to the experimental data, while the open points and dashed lines correspond to RxMC simulations. Key: 573 K (circles), 673 K (diamonds), 773 K (squares), 873 K (triangles). Reprinted with permission from [32]. Copyright 2001, American Institute of Physics.

a one-centre Exponential-6 (Exp-6) potential, which had previously been used to predict thermodynamic properties and liquid–liquid equilibria of helium + hydrogen mixtures. Benzene and cyclohexane were modelled using six-centre Exp-6 potentials, which had previously been used to accurately reproduce saturated liquid and vapour densities, vapour pressures, second virial coefficients, and critical parameters of the six-member ring molecules. No binary adjustable parameters were used to compute the unlike Exp-6 interactions in the ternary system (Lorentz–Berthelot combining rules were used). Simulation results were obtained for a range of temperatures (500–650 K), pressures (1–30 bar), and hydrogen-to-benzene feeds (molar ratios of 1.5:1–6:1). Comparisons of the reaction conversion, molar composition, and mass density of the ternary system were made with calculations using the macroscopic Soave–Redlich–Kwong group contribution equation of state and excellent agreement was found. In [34], Carrero-Mantilla and Llano-Restrepo applied the RxMC method to multiple-reaction vapour-phase equilibria for the hydrogenation of both ethylene and propylene, involving four reactions: $C_2H_4 + H_2 \leftrightarrow C_2H_6$, $C_3H_6 + H_2 \leftrightarrow C_3H_8$, $C_2H_6 + H_2 \leftrightarrow 2CH_4$ and $C_2H_4 + CH_4 \leftrightarrow C_3H_8$. Validated potential models were used: LJ models for hydrogen and methane, quadrupolar 2CLJ models for ethylene, ethane and propylene, and a three-centre LJ model for propane. Again, no binary adjustable parameters were needed to compute the unlike LJ interactions. Effects of temperature and pressure on ethylene and propylene conversion, yield of methane, and density of the system were considered. They considered the effects on the algorithm's efficiency of selecting alternative sets of reactions describing the system. The RxMC results were found to be in very good agreement with calculations using the Soave–Redlich–Kwong group contribution equation of state.

Pusztai et al. [35,36] used results of previous RxMC simulations [25] to test a reverse MC protocol intended to predict concentrations of associating fluid mixtures from experimental structure factor data. The reverse MC method was used to evaluate the features of the local fluid structure, which are consistent with the experimental X-ray diffraction pattern. For this particular study, in lieu of the experimental structure data, reverse MC results were taken as 'exact results' and thus provided a stringent test of the proposed reverse MC protocol. For the dimerisation reaction $2A \leftrightarrow A_2$, Pusztai et al. showed that (under certain conditions) reasonable estimates of the fluid mixture concentrations can be obtained by X-ray diffraction data.

3.2 Combined chemical and phase equilibria simulations and the RGEMC phase equilibrium method

The simulation of combined reaction and phase equilibria was first considered by Johnson et al. [25], who combined the RxMC method with the GEMC technique [67,68]. They computed phase and reaction equilibria for a range of different equilibrium constants for the dimerisation reaction $2A \leftrightarrow B$ and compared their simulations with predictions from a theory for associating fluids. The theory was found to accurately predict the fraction of monomers in the liquid and vapour phases, even when the equilibrium fraction of monomers was very low.

Lísal et al. [37] used the RxMC method to study vapour–liquid equilibria for the $Br_2 + Cl_2 \leftrightarrow 2BrCl$ reacting system. Reacting species were modelled as non-polar and dipolar 2CLJ molecules, where Lorentz–Berthelot combining rules were implemented for unlike atoms. No parameters were fit to any mixture properties in their calculations. The simulated data were compared with experimental results and with previous simulation data obtained by an indirect semi-grand ensemble approach [71–73]. This work demonstrated that the RxMC method is capable of efficiently calculating the complete phase compositions, whereas only a limited subset is available experimentally. The agreement of the simulations with experiment was rather good.

In another work, Lísal et al. [38] applied the RxMC method to a reactive distillation process. They considered reaction and phase equilibria for the isobutene/-methanol/MTBE ternary system along with the reaction *i*-$C_4H_8 + CH_3OH \leftrightarrow$ methyl tertiary butyl ether (MTBE). The system was modelled using the optimised potential for liquid simulations (OPLS) force field [74–77]

without any adjustable binary cross-interaction parameters or mixture data; only vapour-pressure data for the pure components was required as input. To obtain an accurate prediction of the reaction and phase equilibria for these systems, Lísal et al. used modified transition probabilities for the particle transfers. The modified particle-transfer probabilities were developed by Lísal et al. [54,55] within the framework of an approach they called the reaction GEMC (RGEMC) method. The RGEMC approach treats the phase equilibrium conditions as a special type of chemical reaction and incorporates knowledge of the pure-component vapour pressure data into the simulations (which is typically readily available). The modified particle-transfer probability corresponding to Equation (20) becomes

$$P_{kl}^{l\rightarrow v} = \min\left\{1, \Gamma_i \frac{N_i^l V^v}{(N_i^v + 1)V^l} \exp\left(-\beta\Delta U_{kl}^v - \beta\Delta U_{kl}^l\right)\right\}, \tag{28a}$$

for the transfer of particle i from a liquid box into a vapour box, and

$$P_{kl}^{v\rightarrow l} = \min\left\{1, \frac{1}{\Gamma_i} \frac{N_i^v V^l}{(N_i^l + 1)V^v} \exp\left(-\beta\Delta U_{kl}^v - \beta\Delta U_{kl}^l\right)\right\}, \tag{28b}$$

for the particle transfer from a vapour box into a liquid box. In Equation (28), Γ_i is the ideal-gas driving term for the phase-equilibrium reaction i given by

$$\Gamma_i = \frac{P_{i,\text{exp}}^{\text{sat}}}{P_{i,\text{simul}}^{\text{sat}}}, \tag{29}$$

where $P_{i,\text{exp}}^{\text{sat}}$ and $P_{i,\text{simul}}^{\text{sat}}$ are the values of the experimental and simulated vapour pressures of species i (values of $P_{i,\text{simul}}^{\text{sat}}$ can be obtained, for example, from several GEMC simulation runs and then fitted to an empirical expression such as an Antoine equation). Both the non-reacting and reacting isobutene/methanol/MTBE ternary systems were considered over a temperature range of practical interest at a fixed pressure of five bar. Results were compared with calculations from two conventional thermodynamic approaches: the Wilson and UNIFAC free-energy models for the liquid phase, taken together with a truncated virial equation of state for the gas phase in both cases. Simulated results were similar to those of the thermodynamic approaches (see Figures 3 and 4). This work further showed that the RxMC method has advantages over conventional free-energy model approaches since: (i) less experimental data are required for its implementation; (ii) RxMC can also calculate excess internal energies and molar volumes; and (iii) no cross binary interaction parameters are required.

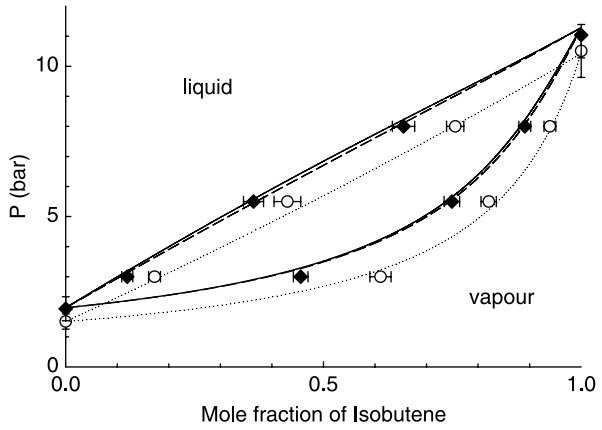

Figure 3. The pressure–composition diagram for the isobutene/MTBE system at 350 K. Open circles and filled diamonds are the GEMC and the RGEMC simulation results, respectively. The solid and dashed lines represent predictions using the Wilson and UNIFAC thermodynamic approaches, respectively. The dotted curves drawn through the GEMC simulation data are guides for the eye only. Reprinted with permission from [54]. Copyright 1999, American Chemical Society.

3.3 Reactions at high temperature: applications to plasma

Plasmas are ideal systems for the application of the RxMC method, since the extreme state conditions do not

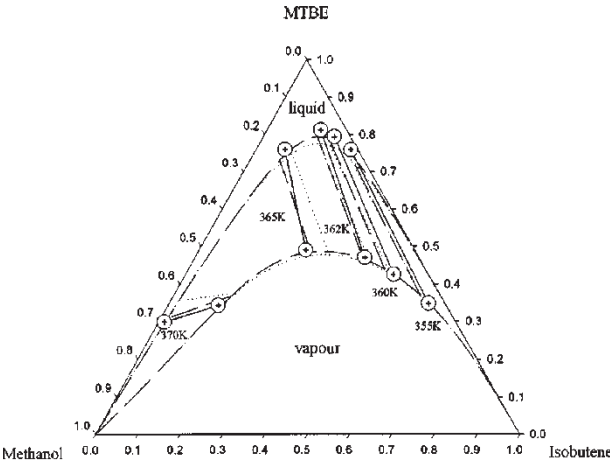

Figure 4. Projection in the ternary composition triangle of the complete reaction and phase-equilibrium diagram for the MTBE ternary system at five bar [38]. Crosses connected by solid lines indicate the reactive tie-lines at a series of temperatures {355, 360, 362, 365, 370} K, as determined by the RxMC simulation results of this work; circles around the crosses denote approximate statistical uncertainties for the simulation results. The dashed and dotted lines represent our predictions of the reaction and phase equilibrium using the Wilson and UNIFAC thermodynamic approaches, respectively. Reproduced with permission. Copyright 2002, American Institute of Chemical Engineers (AIChE).

allow the plasma properties to be assessed experimentally. Temperatures of interest in plasmas range up to 100,000 K, and pressures up to 100 MPa or more. Among the most important properties of a plasma are its composition and thermodynamic properties. Most thermodynamic models of a plasma employ the basic assumption that local chemical reaction equilibria is achieved, implying that the electrons, ions, and neutral particles all have the same (kinetic) temperature. Reaction equilibrium in plasmas at specified (T, P) is attained when the system's Gibbs free energy is minimised subject to mass conservation, charge neutrality, and non-negativity constraints. Sources of non-ideality in plasmas are the long-ranged Coulombic interactions between charged particles, the composition-dependent lowering of the ionisation potential, and the short-ranged particle interactions (neutral–neutral and neutral–charge). Traditionally, only the first two factors have been taken into account in the Debye–Hückel approximate theory.

The RxMC method has been successfully applied to helium [47], argon [48], and air [48] plasmas, with these systems consisting of two, seven and 26 ionisation reactions, respectively. The interactions between charged particles in the plasmas were described by Deutsch's potentials in the form

$$u_{ab}^{Coul} = \frac{z_a z_b e^2}{4\pi\varepsilon_0 r_{ab}}\left[1 - \exp\left(-\frac{r_{ab}}{R_{ab}}\right)\right] + \delta_{ae}\delta_{be}u_{ee}^{s}. \quad (30)$$

In Equation (30), subscript e denotes electrons, r_{ab} is the distance between particles a and b, $R_{ab}^2 = \bar{\Lambda}_a^2 + \bar{\Lambda}_b^2$, where $\bar{\Lambda}_a$ and $\bar{\Lambda}_b$ are the reduced de Broglie thermal wavelengths of particles a and b, given by $\bar{\Lambda} = \hbar/(2\pi m/\beta)^{1/2}$, where $\hbar$ is the reduced Planck constant, and m is the particle mass. Finally, δ is the Kronecker delta. The term u_{ee}^{s} accounts for the electron symmetry effect and is given as

$$u_{ee}^{s} = \frac{\ln 2}{\beta}\exp\left[-\frac{1}{\pi \ln 2}\left(\frac{r_{ee}}{R_{ee}}\right)^2\right]. \quad (31)$$

Both the neutral–neutral particle interactions and the neutral–ion particle interactions were approximated by Exp-6 potentials. In a plasma, the Coulombic interactions lower the ionisation potential of the ions, and the exact calculation of this effect is a complex problem. The essential difficulty is that the internal and configurational parts of the partition function are not independent. As a result, the species thermochemical quantities for the ions in high temperature plasma are composition dependent. These effects were incorporated into the RxMC method using an approximation obtained from the correction of the Saha equation; for details, see [47,48]. Simulations of helium, argon, and air plasmas were carried out over a range of temperatures up to 100,000 K and pressures up to 400 MPa, where plasma compositions (Figure 5), molar enthalpies, molar volumes, molar heat capacities (Figure 6), and coefficients of cubic expansion were

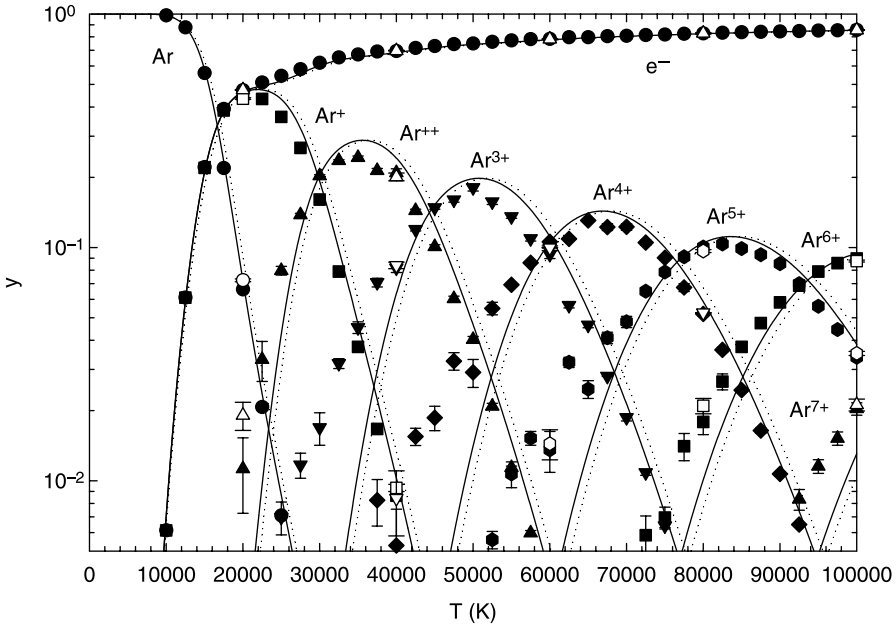

Figure 5. Equilibrium composition of the argon plasma at a pressure of 10 bar, over the temperature range 10,000–100,000 K (filled symbols denote the RxMC simulation results of Lísal et al. [48], with dotted and solid curves corresponding to results obtained using the ideal-gas and Debye–Hückel approximations, respectively). Reprinted from [48], by permission of the publisher (Taylor & Francis Ltd).

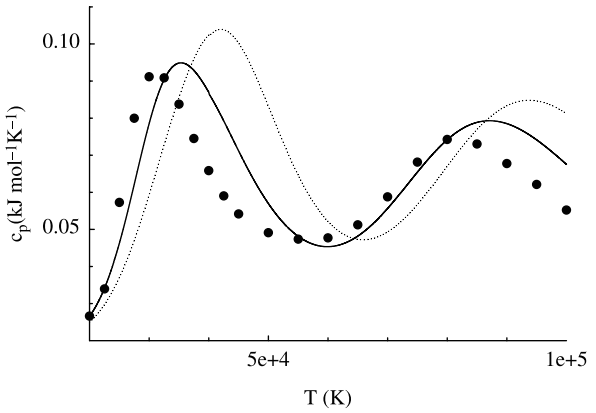

Figure 6. Molar heat capacity of the helium plasma at 400 MPa, over the temperature range 20,000–100,000 K. Filled symbols denote the RxMC simulation results, with dotted and solid curves corresponding to the results obtained using the ideal-gas and Debye–Hückel approximations, respectively. Reprinted with permission from [47]. Copyright 2000, American Institute of Physics.

determined. The simulation results were compared with those obtained using the ideal-gas and Debye–Hückel approximations, and it was found that these approximations were not accurate in comparison with the RxMC results at high pressures.

3.4 Reactions at high pressure: applications to material shock

Several research groups have recently applied the RxMC method to the simulation of the shock Hugoniot properties of materials [50–53]. The Hugoniot curve, a commonly calculated property in shock and detonation science, reveals many properties of shocked materials, knowledge of which is critical to the design of new materials and application platforms. The Hugoniot curve relates the state of the shocked material to its initial unshocked state, and consists of the set of *PVT* points for which the Hugoniot expression:

$$\mathrm{H_g} = e - e_o - \frac{1}{2}(P + P_o)(\nu_o - v), \qquad (32)$$

is zero. In Equation (32), e is the specific internal energy, and $v = 1/\rho$ is the specific volume (ρ is the specific density). The term *specific* refers to the quantity per unit mass, while the subscript o refers to the quantity in the initial unshocked state. Along the Hugoniot curve, the shocked material can begin to chemically react, and therefore, the simulation of the Hugoniot curve must allow reactions to occur. Knowledge of the state conditions at which the Hugoniot curve begins to deviate from the unreacted state is critical to the design of novel energetic materials.

Brennan and Rice applied the RxMC method to determine the shock Hugoniot properties of liquid N_2 and liquid NO [50]. In separate simulation studies, they considered the dissociation reaction of N_2 into atomic nitrogen, $N_2 \leftrightarrow 2N$, and the decomposition of nitric oxide reaction, $2NO \leftrightarrow N_2 + O_2$. For these two simple systems, the RxMC calculations were in excellent agreement with the available experimental data. For the shocked liquid N_2 case (*cf.* Figure 7), Brennan and Rice considered both a reacted and unreacted system, where in the unreacted case the dissociation reaction was ignored. Figure 7 clearly shows that at higher pressures it is critical to include the dissociation reaction to accurately reproduce the Hugoniot curve.

Bezkrovniy and co-workers [51,52] have applied the RxMC technique to study the behaviour of dense hydrogen – a system relevant to a variety of fields including astrophysics, shock physics and, more generally, condensed matter. Their efforts were an attempt to provide a unified description of the behaviour of hydrogen at high pressures, since various experimental and theoretical investigations have yielded inconsistent findings. Application of the RxMC method to the dissociation reaction of hydrogen (and deuterium), $H_2 \leftrightarrow 2H$, resulted in excellent agreement with theoretical predictions and good agreement with experimental measurements.

In one study [51], the authors compared RxMC simulations to theoretical predictions made by combining the hypernetted chain approximation with the mass action law (HNC + MAL). RxMC simulations in the canonical ensemble were performed for a range of

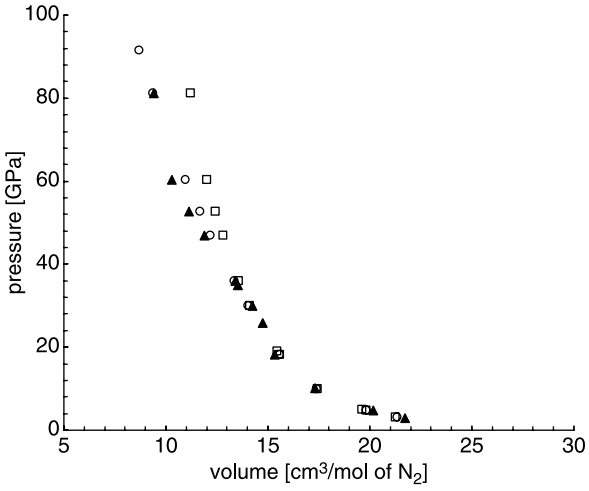

Figure 7. Shock Hugoniot of liquid N_2. Calculated values from RxMC simulations using a reactive (circles) and non-reactive (squares) model are compared with experimental data (triangles) [125,126]. The shock pressure is plotted versus the molar volume of N_2. Reprinted with permission from [50]. Copyright 2002, American Physical Society.

temperatures (2000–20,000 K) and pressures (0–400 GPa) for hydrogen dissociation. Comparison of RxMC simulations and HNC + MAL predictions showed good agreement, providing confidence that the HNC + MAL method can be used to describe shock compressed systems over a wide range of temperatures and densities.

In another study [52], Bezkrovniy and co-workers combined results from the first-principles based direct path integral Monte Carlo technique (DPIMC) and the RxMC method to give the Hugoniot relation over a wide range of densities and pressures. RxMC provided the limiting case of dense hydrogen at low temperatures (less than 15,000 K) where condensed hydrogen consists of atoms and molecules. RxMC simulations accurately describe the Hugoniot curve at lower temperatures where DPIMC simulations become cumbersome, inefficient, and converge poorly since hydrogen is characterised less by pressure ionisation, i.e. ionised plasmas, and more by the formation of molecules. RxMC simulations provided guidance to assessing the theoretical predictions and, combined with DPIMC simulations, provided a unified theoretical picture of dense hydrogen (see Figure 8).

Bourasseau et al. [53] applied the RxMC method to calculate the detonation products along the Hugoniot curve for several prototypical energetic materials, including nitromethane, tetranitromethane, hexanitroethane, pentaerythritol tetranitrate (PETN) and cyclotrimethylene trinitramine (RDX). They determined the point along the Hugoniot curve, known as the Crussard curve, at which the initial material is assumed to have fully decomposed into a mixture of detonation products. In their work, they assumed the following product set: CO_2, H_2O, CO, N_2, H_2, O_2, NO, NH_3 and CH_4. Bourasseau et al. compared their RxMC results to thermochemical calculations [53] and found excellent agreement (*cf.* Figure 9). This work illustrates an important role that the RxMC method can perform in assessing theoretical models used in thermochemical codes such as Cheetah [78] and CHEQ [79]. Bourasseau et al. also developed a fluctuation formula to calculate thermodynamic derivative properties in the reaction ensemble [53]. The formula accounts for fluctuations in energy, composition, and number of molecules, allowing for the determination of properties such as the heat capacity, as well as properties critical to detonation phenomena, including, sound velocities and Grüneisen coefficients.

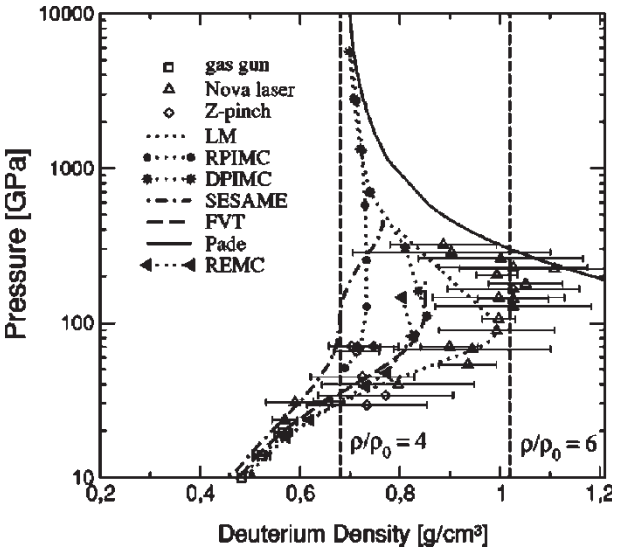

Figure 8. Open symbols and closed symbols indicate experimental measurements and theoretical predictions, respectively; where squares are restricted path integral MC results [127]; circles are *ab initio* MD simulations [128]; and triangles are the combined direct path integral MC and RxMC simulations [52]. See original paper [52] for details of experimental measurements. Reprinted with permission from [52]. Copyright 2004, American Physical Society.

3.5 Reactions under confinement

Another useful application of the RxMC method has been the modelling of molecularly confined chemical reaction equilibria, such as reactions occurring within porous carbons and zeolites. Experimental measurements of chemical reaction equilibria are difficult in these systems. For instance, it is usually impossible to distinguish between true chemical equilibria and long-lived metastable states or to determine the free energy

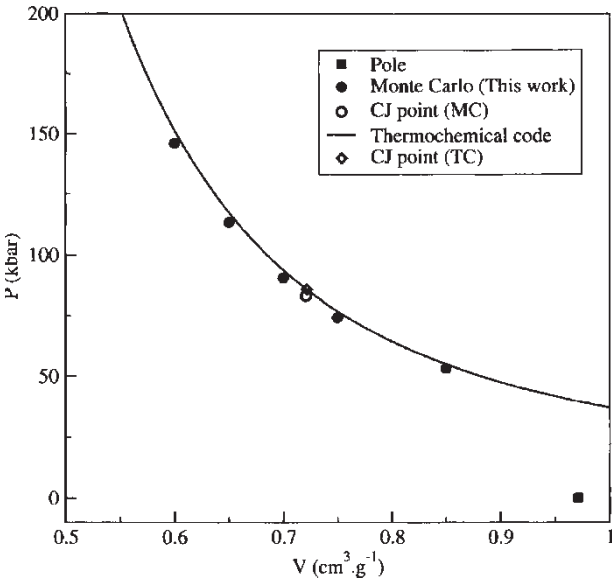

Figure 9. Calculated Crussard curve of PETN. Thermochemical code results from [129]. Reprinted with permission from [53]. Copyright 2007, American Institute of Physics.

of the confined phase. There have been several modelling studies in the literature that have used the RxMC method to determine the composition of a given reaction within a confined geometry.

In one of the initial applications of the RxMC simulation technique, Borówko et al. [42] simulated the conversion of two different model dimerisation reactions near a hard wall and near a LJ wall. They found strong enhancements of the conversion near these walls. Then, just a few years later, Borówko and Zagórski [43] examined the conversion of a LJ dimerisation reaction within a model pore. They found significant shifts of the equilibrium conversion within the pores, and the conversion was found to be sensitive to the pore width and to the strength of interaction with the pore walls (see Figure 10).

In a more realistic system, Turner et al. [32] simulated the equilibrium conversion of the ammonia synthesis reaction ($N_2 + 3H_2 \leftrightarrow 2NH_3$) and the NO dimerisation reaction ($NO + NO \leftrightarrow (NO)_2$) within a model carbon pore, which was in equilibrium with a constant-pressure gas phase [80]. Their results predicted that the conversion of these reactions in the pore would deviate significantly from the bulk phase conversion. The pore was modelled as a slit-shaped carbon pore, and the conversions of the two reactions were found to be strongly affected by the width of the pore (see Figure 11), similar to the general findings of Borówko and Zagórski [43].

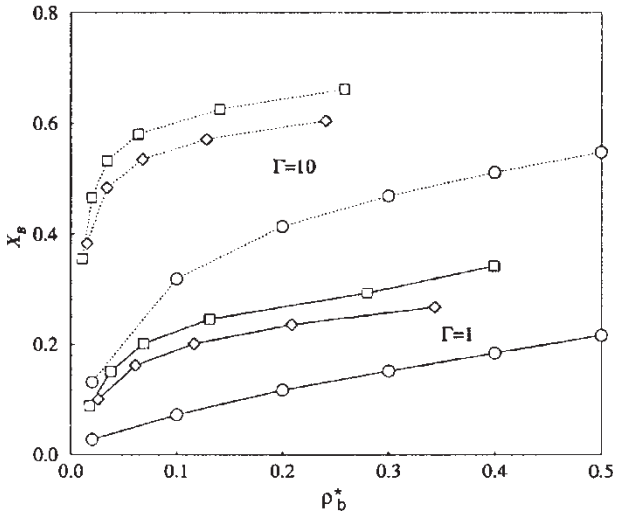

Figure 10. The average mole fraction of the product, X_B, for the reaction $2A \leftrightarrow B$ in pores of width $H = 4$ (squares) and $H = 10$ (diamonds), and for values of $\Gamma = 1$ (solid line) and $\Gamma = 10$ (dotted line), as a function of the equilibrium bulk density ρ_b^*. The circles correspond to results for the corresponding bulk systems. Here, Γ represents the ideal gas equilibrium constant. Reprinted with permission from Ref. [43]. Copyright 2001, American Institute of Physics.

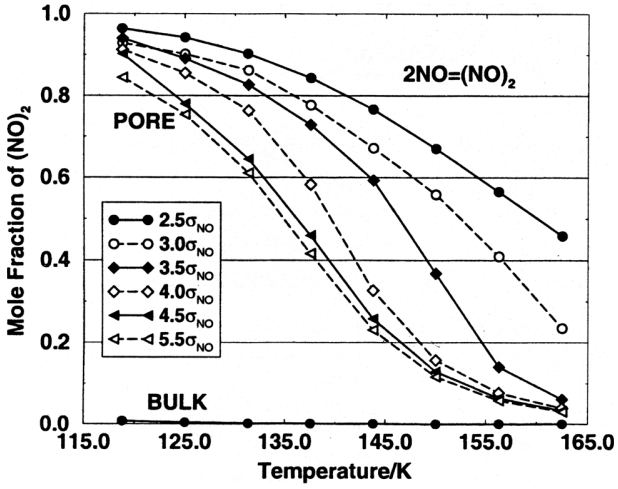

Figure 11. Mole fraction of dimers for the pore phase at a constant bulk pressure of 0.16 bar, for various pore widths expressed as multiples of σ_{NO}, where σ_{NO} is the LJ diameter for the NO molecule (0.3172 nm). Reprinted with permission from [32]. Copyright 2001, American Institute of Physics.

More recently, Lísal et al. [44] expanded the RxMC study of the NO dimerisation reaction in carbon slit pores. They investigated the effects of temperature, pore width, bulk phase pressure, and capillary condensation on the conversion of the pore phase reaction. While the bulk phase pressure had only a small impact on the pore phase conversion, capillary condensation led to dramatic shifts (Figure 12), with a moderate amount of hysteresis predicted in the pore phase conversion. In addition, the authors used the compositions predicted from the RxMC simulations as the basis for a set of MD calculations to determine self-diffusion coefficients of the pore phase mixture (Figure 12(c)).

Related to the NO dimerisation reaction, Tripathi and Chapman [81] used perturbation density functional theory to model the conversion of this reaction within graphitic micropores. The density functional theory calculations used a slightly different potential model. However, the results showed very good agreement with the previous RxMC simulations of this reaction, with respect to the pore phase conversion and the density profiles within the pore, giving further validation to the RxMC approach.

The simulations of reactions in confinement have also been extended to alternate models of the carbon adsorbent [40]. For instance, the ammonia synthesis reaction has also been simulated within bundles of carbon nanotubes, on carbon slit pores chemically modified with functional (carboxyl) groups, and within 'realistic' carbon models. The realistic carbon models were generated using reverse MC by matching experimental structure data [82], yielding an atomistically-detailed carbon model. Interestingly, the simulated conversion within the realistic carbon model was

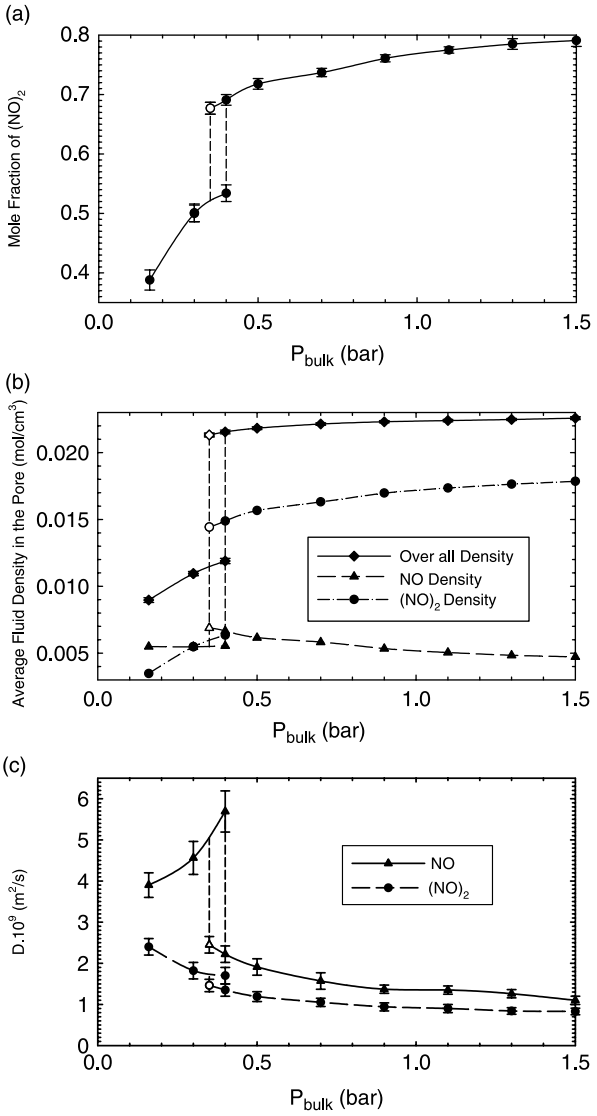

Figure 12. (a) Mole fraction of $(NO)_2$ dimers, (b) average fluid densities in the pore, and (c) one-dimensional self-diffusion coefficients for the NO monomers and $(NO)_2$ dimers, D_{NO} and $D_{(NO)_2}$, as a function of bulk pressure P_{bulk} in the model carbon slit nanopore with a width of 1.7 nm at a temperature of 125 K. The symbols are simulation results of this work and the lines are drawn as a guide to the eye. The adsorption and desorption data points are shown as filled and open symbols, respectively. Reprinted with permission from [44]. Copyright 2006, American Institute of Physics.

accurately predicted by averaging the simulated results in the slit-shaped pore over the pore size distribution corresponding to the realistic carbon. The ammonia synthesis reaction within the functionalised pores was predicted to increase, due to the favourable electrostatic interactions between the polar product (ammonia) and the polar functional groups.

Other studies using the RxMC method have also emphasised the important role of the host structure in catalytic systems. For instance, the propene metathesis reaction system has been studied within zeolite pores in two recent reports [45,46]. In contrast to amorphous carbon materials, zeolites are crystalline materials with well-defined pores, which allow greater control over reaction sensitivity with respect to the host structure. In these two reports, the authors simulated the equilibrium conversion of three simultaneously occurring chemical reactions, involving propene, ethane, *cis*-2-butene, and *trans*-2-butene, where the pore phase was modelled with several different zeolite structures: silicalite-1, MFI, TON, LTL and FER [83]. In conjunction with the RxMC simulation technique, the authors incorporated configurational-bias sampling, in order to improve sampling efficiency. Overall, the authors predicted significant increases in the pore phase conversion, as compared to the bulk phase (Figure 13). In addition, the reaction conversion and selectivity were particularly sensitive to the zeolite pore structure, and the temperature and pressure had a strong influence on the predicted pore-phase composition. The results from these simulations are similar to the experimental measurements of the metathesis reaction, performed by van de Graaf et al. using a silicalite-1 membrane enclosed catalytic reactor [84,85].

3.6 Reactions under solvation and at interfaces

One of the more straightforward applications of the RxMC approach is predicting the conversion of a chemical reaction within different solvents, and some

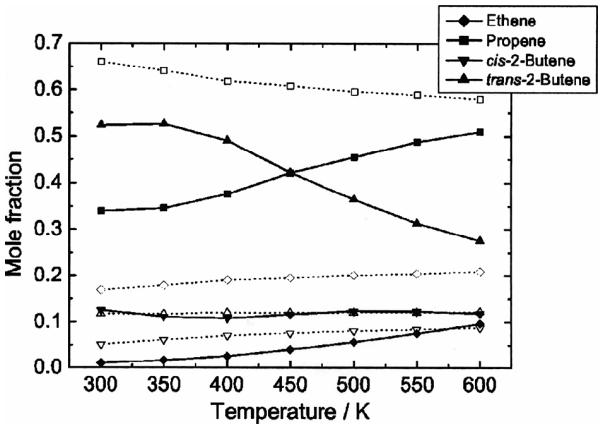

Figure 13. Equilibrium composition in silicalite-1 (filled symbols) determined from GCMC simulations including RxMC trials and particle identity changes. The composition of the bulk reservoir (open symbols) is the chemical equilibrium composition obtained from the isothermal-isobaric ensemble (*NPT*) simulations. Calculations have been carried out at 1 bar bulk pressure. The full and dotted lines are guides to the eye. Reprinted with permission from [45]. Copyright 2005, American Institute of Physics.

of the most prevalent equilibrium-limited industrial reactions are esterification reactions. Along this line, Turner and Gubbins [49] used RxMC simulations to predict the conversion of the esterification of acetic acid (to produce ethyl acetate and water) within a supercritical carbon dioxide solvent and within carbon micropores. Experimentally, the conversion of this reaction is found to be significantly enhanced as the critical point of CO_2 is approached. In the RxMC simulations, this same enhancement was predicted, and from an analysis of the fluid structure, it was apparent that at these conditions there was a significant amount of clustering within the fluid (Figure 14). It was rationalised that the clustering behaviour near the critical point creates a favourable environment for a local enrichment of the product molecules, enhancing the overall conversion. Within the carbon pores, the conversion of the reaction was predicted to double, with a slight dependence on the degree of surface activation (modelled by functionalising the surface with carboxyl groups).

Due to the importance of protein stability to biological and pharmaceutical applications, there is a strong need to develop predictive models for understanding the thermodynamics of protein folding, aggregation, crystallisation, and phase separation. Recently, Cheung and Truskett [57] have used RxMC to predict protein stability in aqueous solutions using a coarse-grained simulation model. They compared the folding behaviour of three different single-domain globular proteins (ribonuclease A, lysozyme, and metmyoglobin) over a range of thermodynamic conditions, in order to understand the experimentally-observed stability of the native-state as a function of the protein concentration. In this work, the authors gathered thermodynamic and structural information from heteropolymer collapse theory [86,87] and then used RxMC simulations to efficiently sample between the folded/unfolded state at various conditions, by treating the folding equilibrium as a chemical reaction. These simulations are able to equilibrate rapidly, since a description of the folding and unfolding processes is unnecessary. Using this approach, the authors were able to predict protein folding behaviour qualitatively consistent with experimental observations, and further work has been performed to develop more detailed information about the protein interactions and phase behaviour [88,89].

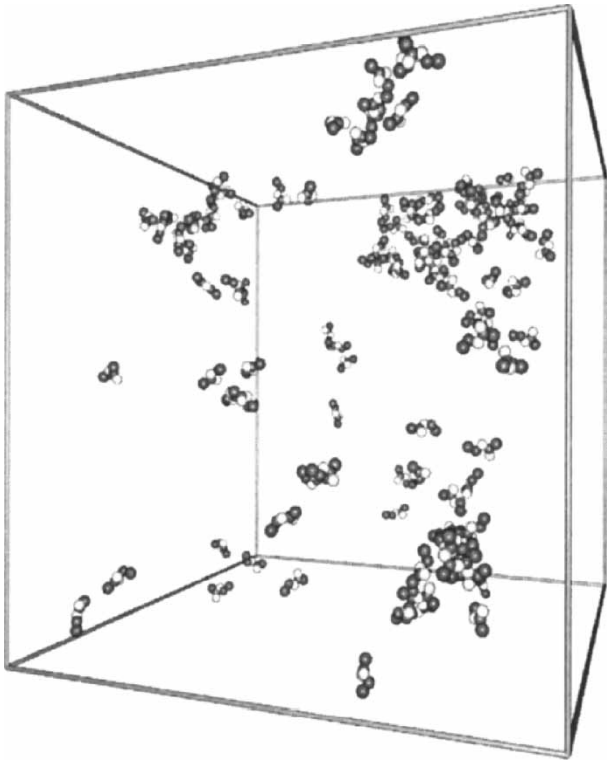

Figure 14. Simulation snapshot of the esterification reaction in 90 mole % CO_2 at 360 K. For clarity, only ethyl acetate molecules are shown. The snapshot shows significant clustering in the fluid. Reprinted with permission from [49]. Copyright 2003, American Institute of Physics.

Chemical reactions are known to be affected at vapour–liquid interfaces, and there have been several experimental and simulation reports in the literature highlighting the possible alterations to reaction kinetics [90]. Much less effort has focused on chemical reaction equilibria within these regions, but two recent examples in the literature have used RxMC simulations to predict reaction conversion at vapour–liquid interfaces [91,92]. In the first study, the equilibrium of an arbitrary reaction $A + A \leftrightarrow B$ was simulated in a two-phase simulation box, which allowed the conversion of the reaction to be simultaneously predicted and compared among the liquid phase, the gas phase, and the vapour–liquid interface. It was found that at the interface, there could be either a strong enhancement or depletion of the reaction conversion, depending upon the intermolecular parameters assigned to the system (Figure 15). An analysis of the system behaviour suggested a relationship between the interfacial tension and the interfacial conversion, and this relationship was then tested and corroborated with additional simulations of realistic reactions, $NO + NO \leftrightarrow (NO)_2$ and $Br_2 + Cl_2 \leftrightarrow 2BrCl$. In the second study, the previous model reaction system ($A + A \leftrightarrow B$) was modified by adding surfactants to the vapour–liquid interface. The surfactants were shown to affect the interfacial tension, and in turn, induce shifts in the interfacial reaction conversion (Figure 16). It was shown that the surfactant characteristics could be tuned to impart varying shifts in the equilibrium conversion at the interface. It is possible that these types of simulations would be beneficial for enhancing current models of atmospheric and aerosol chemistry [93].

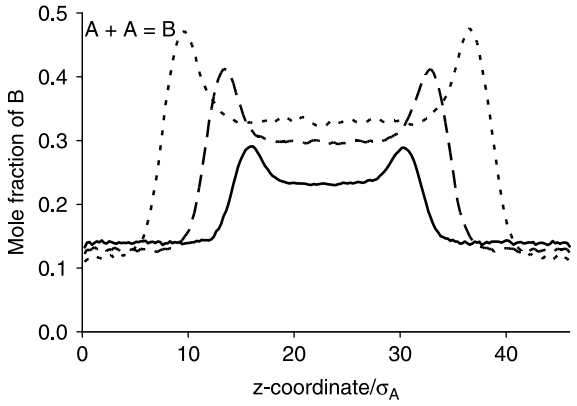

Figure 15. Mole fraction of B (X_B) across the vapour–liquid interface of the A/B dimerisation reaction at a reduced temperature of 0.92. Key: $\sigma_B/\sigma_A = 1.25$ (solid line), $\sigma_B/\sigma_A = 1.50$ (dashed line), $\sigma_B/\sigma_A = 1.75$ (dotted line). Reprinted with permission from [91]. Copyright 2005, American Chemical Society.

3.7 Pressure-induced solid-state phase transitions

RxMC has also been applied to the prediction of solid-state structural transitions, namely conformational polymorphism [56]. In the context of such an application, the RxMC technique provides a means of overcoming high-energy transition barriers, which may be caused, for example, by sterically-hindered atoms or molecules. The ability to simulate such behaviour was demonstrated on crystalline nitromethane (CH_3NO_2) by treating the rotation of the methyl group about the C—N bond as a set of conformational isomerisation reactions (see Figure 17). RxMC was then used to predict the equilibrium concentrations of the rotamers as a function of pressure and temperature. Brennan et al. [56] further showed that

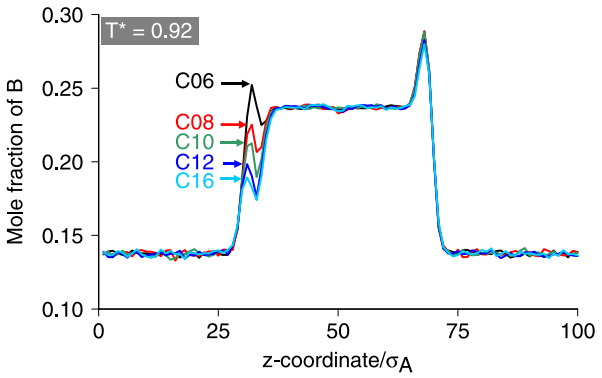

Figure 16. Mole fraction profile across the vapour–liquid interface with the addition of various surfactant models (C06–C16) at a reduced temperature of 0.92. See the original paper [92] for definitions of the surfactant models. For clarity, the curve corresponding to C14 has been removed. Reprinted with permission from [92]. Copyright 2007, American Chemical Society.

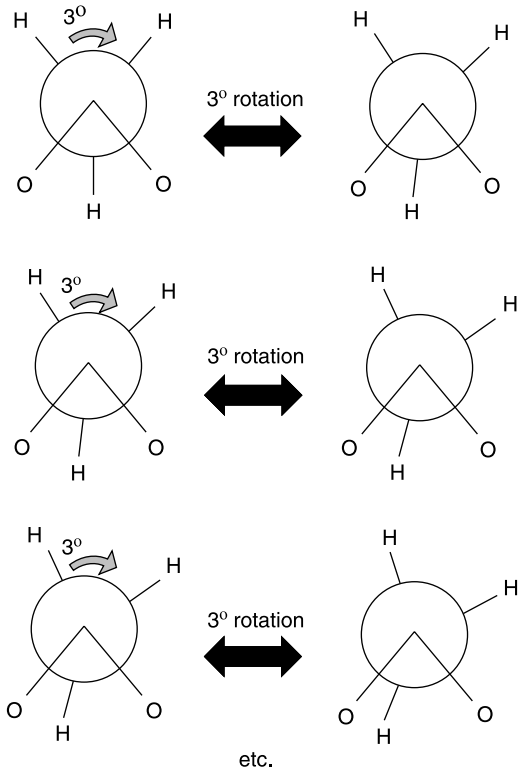

Figure 17. Set of conformational polymorphic reactions used in the RxMC simulations to mimic the methyl group rotation about the C—N bond in crystalline nitromethane. Reprinted with permission from [56]. Copyright 2007, American Chemical Society.

implementing the standard MC method to simulate this type of polymorphic behaviour is not appropriate. To illustrate this, they considered an isothermal-isobaric ensemble MC (*NPT*–MC) simulation that included attempted internal rotations of the methyl group, in addition to the standard MC moves that displace and rotate the molecular centre-of-mass. To mimic the RxMC algorithm and its set of isomerisation reactions, attempted methyl group rotations were constrained to a set of dihedral angles ranging from 0 to 120° in the *NPT*–MC simulation. A comparison of the dihedral angle distributions from such an MC simulation and an RxMC simulation is shown in Figure 18. The discrepancies in the dihedral angle distributions arise because the RxMC algorithm guarantees equilibrium amongst the rotamers, while the *NPT*–MC simulation cannot. Finally, since the acceptance probabilities of the isomerisation reaction set varied considerably in this study, Brennan et al. developed a simple algorithm within the RxMC framework that ensures the number of *accepted* reaction steps is equivalent for each reaction type [56].

It was suggested by Brennan et al. [56] that investigations of other solid-state transitions using the RxMC method could allow for the identification of key

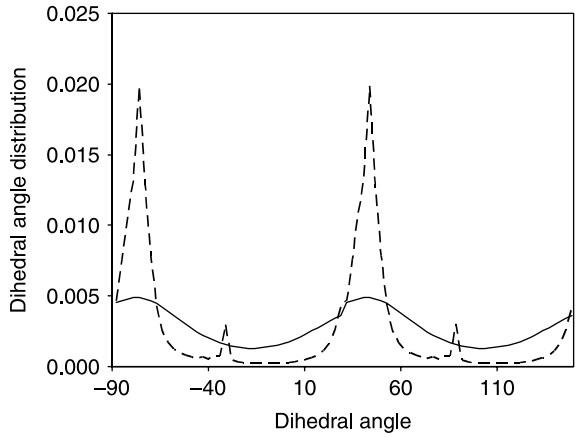

Figure 18. Comparisons of the dihedral angle distributions determined from *NPT*–MC simulations (dashed) and RxMC simulations (solid) for the methyl group rotation in crystalline nitromethane. Reprinted with permission from [56]. Copyright 2007, American Chemical Society.

components of the transition mechanisms through the decoupling of the molecular degrees of freedom. They also suggested that the RxMC method could be a powerful tool in the interpretation of experimental measurements as well as in the confirmation of experimental findings.

4. Extensions of RxMC

Below we review recent extensions and adaptations of the RxMC method beyond the standard applications. These developments include the simulation of kinetics, the transport properties of reacting mixtures in porous solids, constant internal-energy or constant–enthalpy systems, and mesoscale simulations of chain molecules.

4.1 Transition state – RxMC

RxMC simulations have been traditionally used to predict the overall equilibrium of a chemical reaction, and the acceptance criteria for the reaction moves used in these simulations are based on the overall free energy of the reaction at a standard state. The effects of the surrounding environment on the reaction are included with intermolecular potentials, such as LJ and electrostatic interactions. This general approach to predict equilibrium conversion can also be applied to predict chemical reaction kinetics, within the context of transition state theory, and this implementation has been referred to as TS-RxMC [22]. Within the approximations of canonical transition state theory, it is assumed that there is a quasi-equilibrium between the reactants and the transition state species (instead of the product species in an equilibrium-limited reaction), given several general approximations [94–97]. Conventional TST is further based on the assumption that the activation barrier, ΔE^*, is large compared to the thermal energy of the molecules (a rule of thumb is $\Delta E^* > 5k_BT$), so that barrier re-crossings are rare. The equilibrium between the reactants and the transition state is governed by the activation barrier, which can be approximated with quantum mechanical calculations or estimated experimentally. In a TS-RxMC simulation, the relative concentrations of the reactants and transition state species are estimated. These concentrations are affected by the standard-state activation barrier (an input parameter) and the intermolecular interactions present in the simulations. The relative concentrations of the reactants ($[A_1]$–$[A_{NR}]$) and transition state species ([TS]) can be used to quantify shifts in the chemical reaction kinetics in different environments according to

$$k = \kappa \frac{k_B T}{h} \frac{[\mathrm{TS}]}{[A_1]\cdots[A_{NR}]}. \tag{33}$$

In this equation, κ accounts for any re-crossing of the transition-state barrier, and h is Planck's constant.

The TS-RxMC formalism can be used to identify how reaction kinetics can be changed within confined structures. For example, the transition state for a particular reaction may become geometrically constrained in a confined environment, significantly reducing the probability of forming the transition state and ultimately degrading the reaction kinetics. Alternatively, certain constraints may favour the formation of the transition state, and hence, increase the rate of a particular reaction. Using this approach, Turner et al. [22] predicted enhancements of almost two orders of magnitude in the reaction rate of a model reaction, when the reaction was confined within carbon nanotubes, since the geometry of the transition state strongly favoured this particular environment.

4.2 RxMC at fixed total internal energy or enthalpy

Simulations of the properties of reactive fluid systems at fixed total internal energy U or at fixed total enthalpy H are important problems of both theoretical and practical interest. Two examples are: (i) detonations at specified (U, V); and (ii) adiabatic reaction temperature and composition calculations at specified (H, P). For such problems, the main objective is to calculate the system temperature along with other system properties.

Simulations at fixed U or H for non-reactive systems were first considered by Graben and Ray [98], and later by Kristóf and Liszi [99]. However, they developed approaches that perform a simulation at a specified value of the sum of the system kinetic energy and the configurational energy, and at a specified value of the sum of these quantities and PV. The system kinetic energy corresponds to $(f/2)N/\beta$, where f is the number

of degrees of freedom per particle. However, the specified quantities do *not* correspond to the total internal energy and total enthalpy, respectively. This is because in the case of atomic fluids, the electronic and nuclear energy-level contributions to the system's ideal-gas energy U^{IG} are not included. Likewise, in the case of molecular fluids the vibrational, electronic, and nuclear energy-level contributions to U^{IG} are also not included (rotational energy levels are treated approximately).

To circumvent this issue, Smith and Lísal [58], and Lísal et al. [100] developed an approach that allows the total U or total H to be fixed in simulations. The method is applicable to both non-reacting and reacting (in conjunction with the RxMC technique) fluid systems in single or multiple phases. The method considers a MC step for a change in the inverse temperature $\Delta\beta = \beta_l - \beta_k$, in addition to standard particle displacements/reorientations, reaction moves, volume changes (for constant-P simulations), and inter-phase particle transfers (for multiple phase simulations). The trial β changes are accepted with probability [58,100]

$$P_{kl}^{\beta} = \min\left\{1, \exp\left[\left(U_k^{IG} + U_k - U^*\right)\Delta\beta\right]\right\}, \qquad (34)$$

for a simulation at fixed (U, V) and

$$P_{kl}^{\beta} = \min\left\{1, \exp\left[\left(H_k^{\mathrm{IG}} + U_k + P^* V_k - \frac{N}{\beta_k} - H^*\right)\Delta\beta\right]\right\}, \qquad (35)$$

for a simulation at fixed (H, P). In the above equations, the superscript (*) denotes the specified input value. The ideal-gas values U^{IG} or H^{IG} are conveniently obtained from tabular compilations of thermochemical data [64,65] with the definitions

$$H^{\mathrm{IG}} = \sum_i \frac{N_i}{N_{\mathrm{A}}} h_i^{\mathrm{IG}} \qquad (36a)$$

$$h_i^{IG} = \Delta H_{fi}(298.15) + \int_{298.15}^{T} c_{Pi}(T)\mathrm{d}T \qquad (36b)$$

$$U^{\mathrm{IG}} = H^{\mathrm{IG}} - \frac{N}{\beta}, \qquad (36c)$$

where ΔH_{fi} is the molar enthalpy of formation of species i, c_{Pi} is its molar heat capacity, and N_{A} is Avogadro's constant.

The RxMC method at specified (H, P) was applied by Lísal et al. [101] to the industrially-important ammonia synthesis reaction in an adiabatic plug-flow reactor. They performed direct simulations of the equilibrium reaction temperature and the composition of the exit stream as a function of the temperature and pressure of the inlet stream. The reacting species were modelled by all-atom potentials. They compared the simulation results with experimental data and with a thermodynamic model based on the Soave–Redlich–Kwong equation of state (Figure 19). The simulation results for the reaction conversion showed very good agreement with the available experimental data over a wide range of temperatures and pressures, whereas the corresponding results for the thermodynamic model slightly deteriorated with increasing pressure.

4.3 Dual control cell reaction ensemble molecular dynamics

Confinement contributes significantly to the thermodynamic and transport properties of fluids if reactions and phase separation occur simultaneously in porous materials. Lísal et al. [60] developed a simulation tool that allows for the study of fluid mixtures that are simultaneously chemically reacting and adsorbing

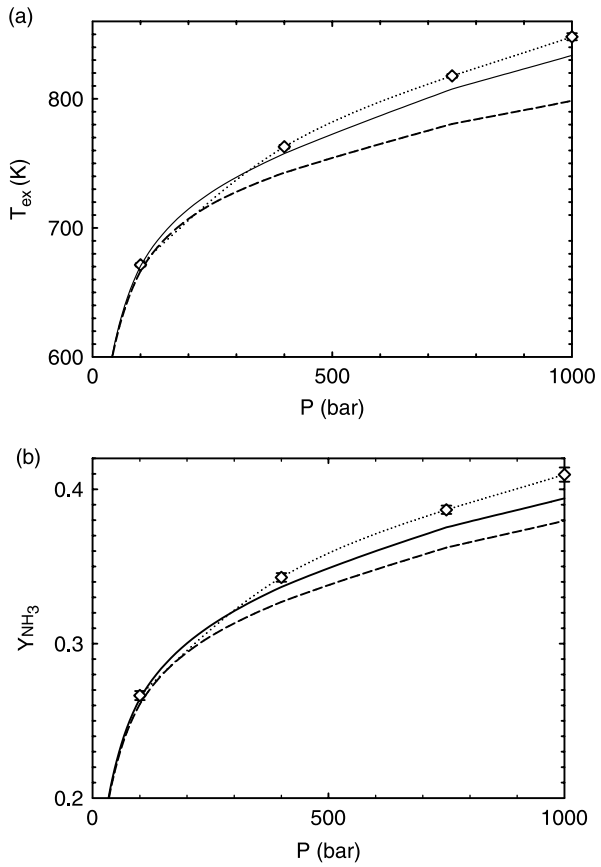

Figure 19. (a) Adiabatic reaction temperature T_{ex}, and (b) equilibrium ammonia yield $y_{\mathrm{NH_3}}$ as a function of pressure P for a non-reacting inlet stream consisting of a stoichiometric mixture of N_2 and H_2 (1:3) at the inlet temperature 298.15 K. The diamonds are the (H, P) RxMC simulation results of Lísal et al. [101], with the dotted line serving as a guide to the eye only. The dashed and solid lines correspond to results calculated from the ideal-gas and Soave–Redlich–Kwong thermodynamic models, respectively. Reprinted from [101], Copyright 2005, with permission from Elsevier.

in a nanoporous material. The method is a combination of the RxMC technique and the dual control volume grand canonical MD method [102,103]. The method, termed the dual control cell reaction ensemble molecular dynamics method (DCC-RxMD), allows calculation of both equilibrium properties and non-equilibrium transport properties in nanoporous materials such as diffusion coefficients, permeability and mass flux. Control cells, which are in direct physical contact with the porous solid, are used to maintain the desired reaction and flow conditions for the system. The simulation set-up closely mimics an actual experimental system in which both the thermodynamic and flow parameters are precisely controlled.

To mimic reaction and adsorption mechanisms in a nanoporous material, the DCC-RxMD method considers a simulation box as shown in Figure 20. A membrane of thickness δ is placed at the centre of the simulation box. The left-hand-side of the simulation box with reaction control cell I corresponds to a reaction void of a real nanoporous material, while the right-hand-side of the simulation box with transport control cell II corresponds to a transport void of a real nanoporous material. The DCC-RxMD method imposes periodic boundary conditions in both the *y* and *z* directions since it is assumed that the sizes of the reaction and transport voids in these directions are much larger than the membrane thickness. The reaction equilibrium in control cell I is controlled by the RxMC method, and the trajectories of the fluid particles within the entire DCC-RxMD simulation volume are generated by the MD simulation method. In order to maintain a flux of particles through the membrane, the DCC-RxMD method imposes a pressure gradient across it. The pressure gradient is indirectly controlled by performing GCMC particle insertion and deletion steps in control cell II (the transport void) only. For such a set-up, the DCC-RxMD simulation proceeds as follows. After n_{MD} MD steps, the system is frozen, i.e. particle positions are held fixed, and the DCC-RxMD performs n_{RxMC} forward and reverse reaction moves in control cell I, and n_{GCMC} particle creation and destruction steps in control cell II. Both the RxMC and GCMC algorithms require insertion of particles into the control cells. The velocities for the inserted particles are assigned from a Maxwell–Boltzmann distribution corresponding to the specified *T*. Values of n_{MD}, n_{RxMC} and n_{GCMC} must be chosen appropriately to maintain reaction equilibrium in control cell I, constant chemical potentials in control cell II, and reasonable transport rates at the boundaries between the control cells and the membrane region.

The DCC-RxMD method was applied to the dry reforming of methane reaction (see Figure 21) within

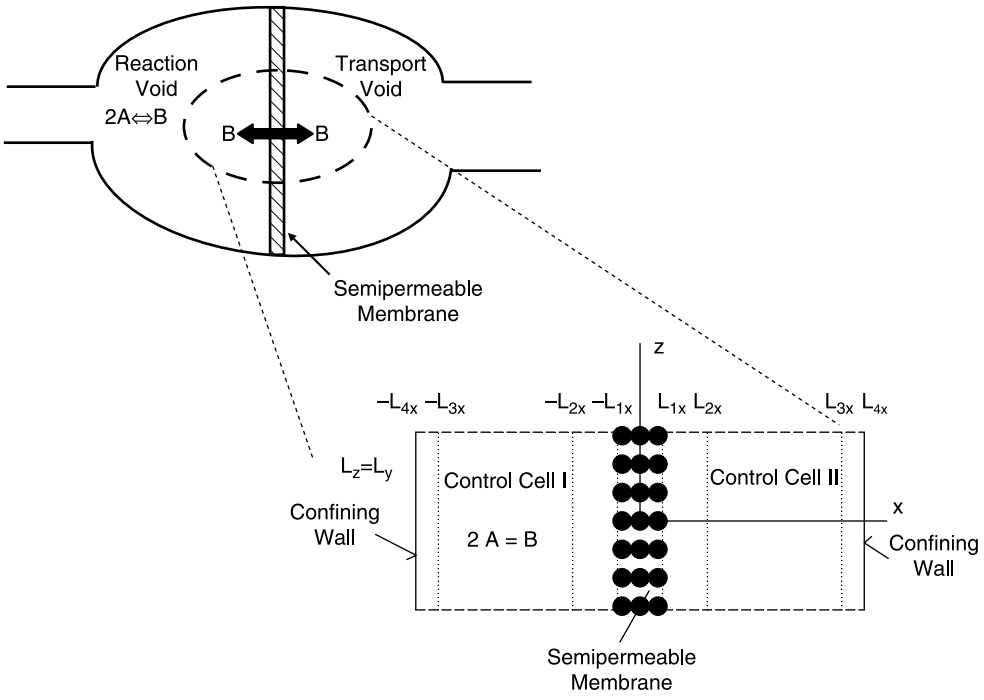

Figure 20. Schematic of a DCC-RxMD simulation box comprised of a reaction control cell I and a transport control cell II separated by a semi-permeable membrane. A model reaction 2A ↔ B takes place in the reaction control cell I while component B is separated via the semi-permeable membrane. Periodic boundary conditions, applied in both the *y* and *z* directions, are omitted in the *x*-direction due to the presence of repulsive confining walls (in the *yz*-plane) at each end of the simulation box. Reprinted with permission from [60]. Copyright 2004, American Institute of Physics.

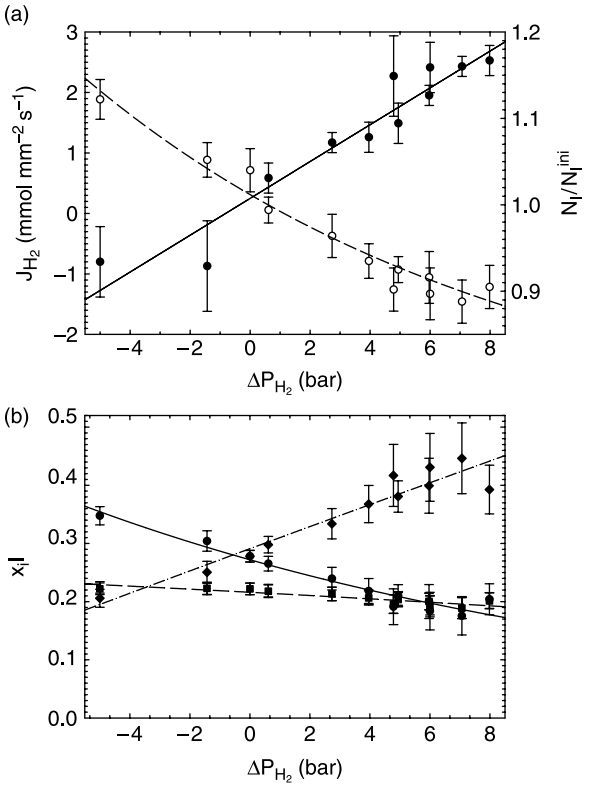

Figure 21. (a) Hydrogen molar flux J_{H_2} (●), and N_I/N_I^{ini} (○) as a function of the hydrogen partial pressure difference ΔP_{H_2} and (b) the composition in the reaction void x_i^I (CH_4, □; H_2,○; CO,◇) as a function of ΔP_{H_2} in the case of Powles' membrane obtained from the DCC-RxMD simulations. Due to identical initial compositions of CH_4 and CO_2, $x_{CH_4}^I = x_{CO_2}^I$ (within statistical uncertainties), $x_{CO_2}^I$ is not plotted. The lines serve as a guide to the eye only. Reprinted with permission from [60]. Copyright 2004, American Institute of Physics.

a nanoscale reactor model in the presence of a semi-permeable membrane that was modelled as a nanoporous material similar to silicalite [60,104]. In [60] and [104], the authors studied the effects of the membrane structure and porosity on the permeability of the reaction species by considering three different membrane models. They also studied the effects of an imposed pressure gradient across the membrane on the mass flux of the reacting species. Conversion of syngas (H_2/CO) increased significantly for all nanoscale membrane reactor models considered in the study.

4.4 Reaction ensemble molecular dynamics

An extension of the RxMC method that is a more general application of the DCC-RxMD is called the reaction ensemble molecular dynamics method (RxMD) [59]. Similar to the DCC-RxMD, RxMD combines the RxMC method with constant-temperature MD. The method can be used to calculate the equilibrium transport properties of reacting mixtures that cannot be determined by using the RxMC method alone. A schematic of the RxMD method is shown in Figure 22. To avoid disruption to the deterministic pathway of the particle trajectories, the total simulation cell is partitioned into a set of control cells and a dynamic cell positioned between these control cells. A model reaction system, $2A \leftrightarrow B$, is shown in Figure 22, where MD time steps are performed in all three cells while reaction steps are performed in the control cells only. Since the control cells are in direct contact with the dynamic cell, the particles are able to move freely amongst all three cells. The properties of the dynamic cell (which is extended in the *x*-direction relative to the control cells) are calculated from an interior portion of the dynamic cell (shown as dashed lines in Figure 22). The interior portion of the dynamic cell should be as far away from the control cell-dynamic cell interfaces as possible in order to minimise differences in the thermodynamic states (i.e. species concentrations) between the cells. Thermodynamic and transport properties are calculated in the dynamic cell by using the constant-temperature MD method [66], while a number of RxMC reaction steps are performed between MD displacement steps to ensure that the control cells are maintained at the system conditions. Note that due to periodic boundary conditions, the control cells on either side of the dynamic cell behave as a single, continuous cell. Also note that the dynamic properties that are calculated are more precisely dynamic *equilibrium* properties since they describe correlations at different times along an equilibrium trajectory [66]. Finally, note that analogous to the RxMC method, RxMD predicts the *physical* effects on reaction equilibria as opposed to predicting *chemical* effects, and furthermore, no reaction rate information can be gained directly from an RxMD simulation. Despite these limitations, the RxMD method can provide unique insight into the molecular-level dynamic behaviour of a wide variety of reacting systems. RxMD appears most appropriate when reaction rates are very fast relative to diffusion events, so that reaction and thermodynamic equilibrium is assumed to be maintained at each point in the system.

At this point, it is worth noting a few fundamental differences between the RxMD method and the DCC-RxMD method described in Section 4.3. Analogous to the DCC-RxMD approach, the RxMD method can also be applied to the study of inhomogeneous fluids, e.g. fluids confined in nanoporous materials or membranes, by incorporating a porous model into the dynamic cell. However, while the RxMD method can be applied to both homogenous and inhomogeneous systems, the control cells remain at identical thermodynamic conditions via the RxMC method. Contrastingly, the two control cells in the DCC-RXMD method can be maintained at different

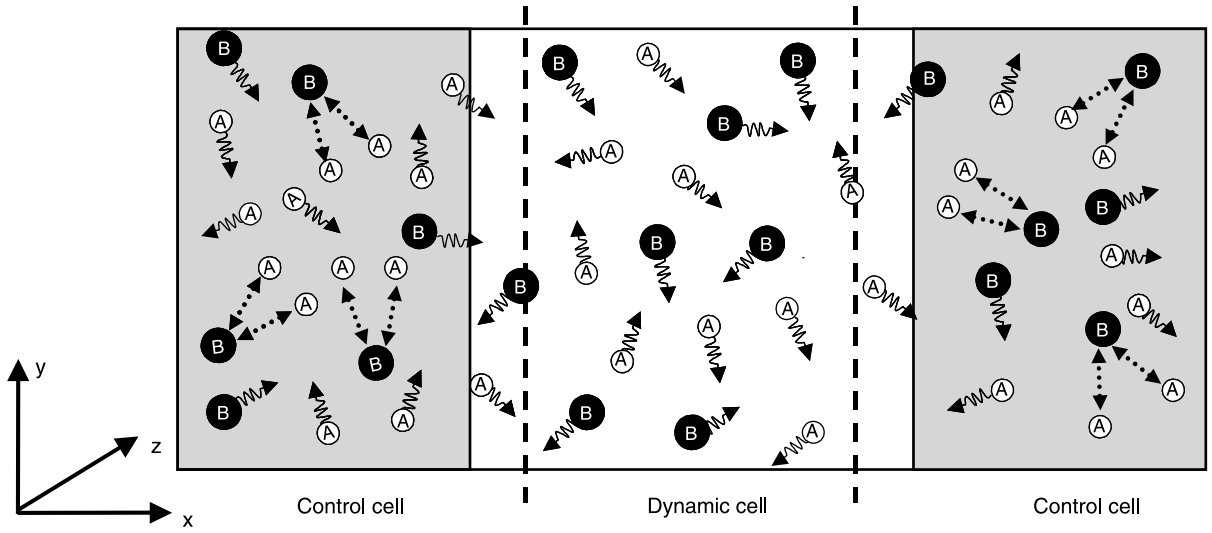

Figure 22. Schematic of the reaction ensemble molecular dynamics method. The model reaction, 2A ↔ B is occurring. MD particle displacement steps (solid trajectories) occur in all three cells, while RxMC reaction steps (dotted arrows) occur only in the control cells. The dashed lines denote the portion of the dynamic cell in which the dynamic properties are calculated. Reprinted with permission from [59]. Copyright 2004, American Physical Society.

thermodynamic conditions via the RxMC and GCMC methods, respectively. A DCC-RxMD simulation would reduce to an RxMD simulation if both control cells were maintained at the same thermodynamic conditions. In such a case, the confining walls in the DCC-RxMD schematic (Figure 20) would be unnecessary. Finally, note that the gradient imposed by the control cells in the DCC-RxMD method drives fluid flow through the porous material, allowing for both equilibrium and non-equilibrium transport properties to be determined.

4.5 Cavity bias – RxMC

A few adaptations of the RxMC method that address phase space sampling difficulties have been developed. One of the adaptations, mentioned previously in Section 3.7, was an algorithm that adjusts the sampling probabilities for each reaction type in a multi-reaction system, with the goal of achieving equality of the acceptance probabilities. This algorithm has been shown to enhance sampling efficiency for RxMC simulations that contain multiple reactions with disparate reaction step acceptance probabilities [56]. Two other adaptations have been developed to overcome poor sampling, which may be caused by energetically-unfavourable conditions during the product molecule insertion step. In one of these possible solutions, a cavity-bias sampling algorithm [105–107] was developed for the RxMC method, denoted as CB-RxMC [23]. Akin to other biasing schemes that are implemented into insertion-based MC methods, such as GEMC [107], CB-RxMC searches for unoccupied space in the reacting mixture whereby the insertion of a product molecule is more energetically favoured. This sampling bias is then corrected in the acceptance criteria. Implementation of the CB-RxMC algorithm allows for the study of reacting mixtures at high density, which are not feasible with conventional random sampling. For a given state point, the efficiency of the CB-RxMC technique depends on the number of trial insertions (k_i) for each attempted reaction step. A computational tradeoff exists between the additional expense of generating k_i configurations and the overall phase space sampling efficiency (see Figure 23). A simple approach

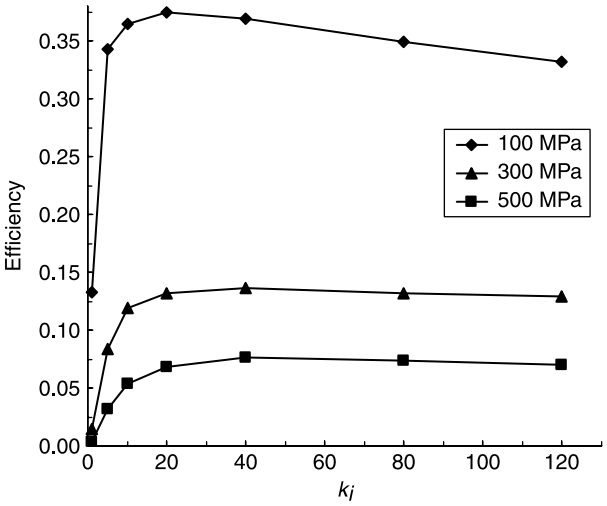

Figure 23. Efficiency of the CB-RxMC algorithm as a function of the number of trial insertions for the $2H_2O + C_2H_4 \leftrightarrow 2CO + 4H_2$ reaction at different pressures. Line is shown as a guide to the eye only. Reprinted from [23], by permission of the publisher (Taylor & Francis Ltd).

was suggested for optimising the value of k_i. In the original paper [23], the method was shown to increase the efficiency of the reaction steps by a factor greater than 20 in some of the cases considered. CB-RxMC can be readily generalised to other biasing schemes, such as orientation-biasing of polar molecules and configuration-biasing of polyatomic and chain-like molecules. The CB-RxMC algorithm has been implemented recently in the simulation of the Hugoniot curve for nitromethane [108], while a similar method has been utilised recently to map out the Crussard curve of nitromethane [53].

4.6 *Replica exchange for RxMC*

In general, when configuration sampling becomes challenging in a molecular simulation, one of the recent solutions is to apply the replica exchange technique [109,110]. This approach simultaneously simulates multiple non-interacting replicas of a given system, and periodically exchanges configurations among the replicas. Typically, the temperature is incrementally varied among the replicas, so that the configuration swaps with higher temperature replicas allow the system to easily escape local minima energy traps. This approach allows phase space to be more efficiently sampled, and it has been successfully applied to many systems within the last few years [110–117].

Recently, the replica exchange technique has been applied to RxMC simulations; it was abbreviated as RE-RxMC [24]. The acceptance criterion for a configuration swap between replicas labelled 'A' and 'B' is shown below, while the forward and reverse reaction steps within each replica follow the standard RxMC acceptance rules.

$$P^{\text{swap}} = \min\Big\{1, \exp\Big[-\beta_{\text{A}}\Delta U_{\text{A}}(x_{\text{BA}}) - \beta_{\text{B}}\Delta U_{\text{B}}(x_{\text{AB}}) - \delta\xi\left(\frac{\Delta G_{\text{A}}^{\circ}}{RT_{\text{A}}} - \frac{\Delta G_{\text{B}}^{\circ}}{RT_{\text{B}}}\right) + \delta\xi \ln\left(\frac{V_{\text{B}}T_{\text{A}}}{V_{\text{A}}T_{\text{B}}}\right)\Big]\Big\} \quad (37)$$

Here, $\Delta U_i(x_{ij}) = [U_i(x_i) - (U_i(x_j)]$ and $\beta_i = 1/(k_{\text{B}}T_i)$, where the $U_i(x)$ term represents the potential energy of configuration x calculated with the intermolecular potential assigned to replica i. The variable ΔG_i°, represents the ideal-gas standard free energy at reference pressure P° of the reaction within replica i, V_i is the volume of replica i, and $\delta\xi$ is used to account for the difference in the extent of conversion among the two replicas

$$\delta\xi = \frac{N_i(x_{\text{B}}) - N_i(x_{\text{A}})}{\nu_i}. \quad (38)$$

RE-RxMC simulations require slightly more finesse than replica exchange simulations in other ensembles. This is due to the fact that incrementing the temperature (or other parameters) among the replicas can induce dramatic shifts in the equilibrium conversion within each replica, and dissimilar conversions among the replicas cause the acceptance probability for the configuration swaps to become very small. However, it is possible to temper other variables, as well, and this can substantially increase the swap acceptance probability. In [24], the authors use the RE-RxMC technique to significantly improve the MC sampling within a high-density fluid. This is accomplished by incrementally reducing the magnitude of the intermolecular potential within the replicas (which improves sampling) and simultaneously scaling the reaction free energy within each of the replicas, in order to maintain the equilibrium conversion within each replica close to that of the central image. While the RE-RxMC method is not a straight-forward approach, in challenging cases, it can be used to improve sampling efficiency by two or three orders of magnitude (Figure 24).

4.7 *Reaction ensemble dissipative particle dynamics*

Recent advances in polymer synthesis techniques have enabled polymers to be functionalised with one or more bonding groups that can each form a reversible linkage of precise functionality with another bonding group. The functionalised polymers then bond together to form supramolecular polymers of various architectures. For example, supramolecular diblock copolymer systems

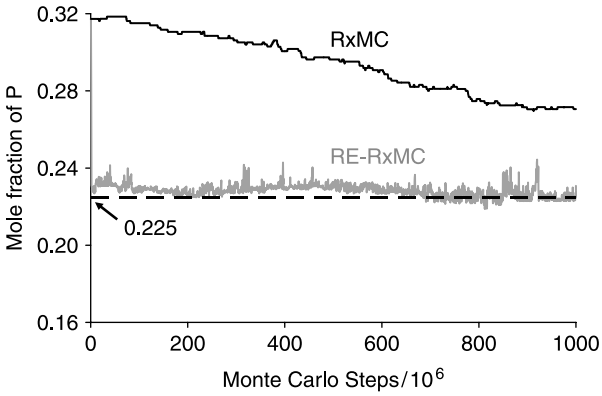

Figure 24. RxMC versus RE-RxMC simulation results at $T^* = 3.0$ and $\rho_T^* = 0.69$ with $\delta_\kappa = -0.03$, $\delta\Delta G_{\text{AB}}^{\circ} = 0.83$, and $M = 13$, where T^* is the reduced temperature, ρ_T^* is the reduced density, δ_κ is the intermolecular potential scaling factor, $\delta\Delta G_{\text{AB}}^{\circ}$ is the reaction free-energy scaling factor, and M is the number of replicas (*cf.* [23] for details). For clarity, only the central replica of the RE-RxMC simulation is shown (solid grey line), along with the mole fraction from the standard RxMC simulations (solid black line), and the final equilibrium average (dashed black line). Reprinted with permission from [24]. Copyright 2007, American Chemical Society.

consist of chemically-incompatible homopolymers A and B with terminal hetero-complementary bonding groups that can reversibly bind to form AB diblock copolymers. The reversible nature of the linkage between bonding groups implies that an external field, e.g. temperature, can be used to control the average size and architecture of the supramolecular polymers, and hence, the system properties such as the viscosity. To simulate such phenomena, the reversible linkage can be treated as a chemical reaction, for example as A + B ↔ AB for the supramolecular diblock copolymer system. The average chain length and architecture of the supramolecular polymers directly depends on the reaction equilibria behaviour. The length and time scales of the formation of supramolecular polymers are beyond the scope of atomistic simulations so one must rely on coarse-grained, particle-based mesoscale models, such as soft bead-spring models that retain only the most essential features of the system.

Recently, Lísal et al. [61] proposed a mesoscale simulation technique, called the reaction ensemble dissipative particle dynamics method (RxDPD), for studying the reaction equilibria of polymer systems. The RxDPD method combines elements of dissipative particle dynamics (DPD) [118–121] and RxMC, allowing both static and dynamic properties of a polymer system to be determined. An RxDPD simulation of polymers contains full polymer chains, and depending on the type of reaction being simulated, a certain number of fractional polymer chains, i.e. polymer chains with fractional DPD particles. These fractional particles are coupled to the system via a coupling parameter λ that varies between zero (no interaction between the fractional particles and the other particles in the system) and one (full interaction between the fractional particle and the other particles in the system). For example, in the case of the supramolecular diblock copolymers, the system contains (in addition to full A, B, and AB polymers) two fractional polymers (see Figure 25): one fractional polymer, either fA or fB, and another fractional polymer, fAB [122]. The time evolution of the system is governed by the DPD equations of motion, accompanied by changes in λ. Changes in λ, which mimic forward and reverse reaction steps, are either accepted with a probability derived from the grand canonical partition function or governed by an equation of motion derived from the extended Lagrangian [123].

The utility of the RxDPD method was first demonstrated on several simple polydispersed homopolymer systems [61]. The polydispersity was not specified in these simulations; rather, it was predicted using the following set of polymerisation reactions

$$A_i \leftrightarrow A_{i+1} \quad (i = 1, 2, \ldots, \infty), \tag{39}$$

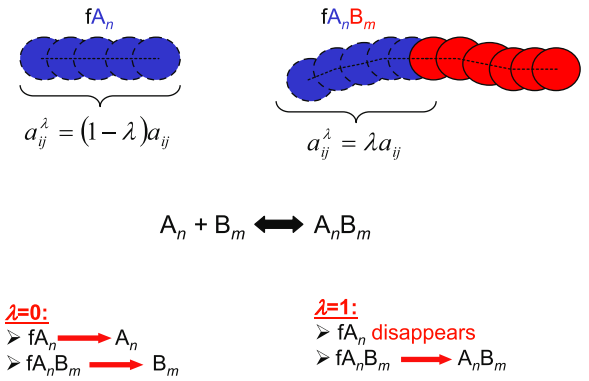

Figure 25. Fractional polymers fA$_n$ and fA$_n$B$_m$ for the mesoscale simulation of supramolecular diblock copolymer systems. The subscripts n and m denote the number of DPD beads of homopolymers A and B, respectively; λ is the coupling parameter and a_{ij} is the maximum repulsion between particles i and j. Note that for $\lambda = 0$, fA$_n$ and fA$_n$B$_m$ become the full A$_n$ and B$_m$ homopolymers, respectively, while for $\lambda = 1$, fA$_n$ disappears from the system and fA$_n$B$_m$ become the full A$_n$B$_m$ diblock.

where A$_i$ and A$_{i+1}$ denote polymers of lengths i and $i + 1$, consisting of i and $i + 1$ DPD particles, respectively. Currently, Lísal et al. [122] are applying the RxDPD method to the simulation of supramolecular diblock copolymer systems.

5. Discussion

From this review, it is clear that the RxMC method is a powerful simulation tool for studying reacting mixtures. Its primary utility is for efficiently predicting shifts of reaction equilibria caused by non-ideal environments. RxMC can be considered as a complementary tool to the various other computational approaches that are available [10], such as *ab initio* calculations. Taken together, these tools can provide a more complete description of the phenomena occurring in chemically reacting systems. We saw that RxMC can be applied to a wide scope of reacting systems, and it is our hope that this review provides motivation to apply it further. Other applications might include gelation studies, atmospheric chemistry, and electrochemistry, for example, a strategy for the prediction of aqueous electrolyte solubility based on a combination of the RxMC and MD methods was recently presented by Lísal et al. [124]. Still other applications could include reactions involving condensed phases, such as carbon cluster formation which often occurs during detonation and combustion processes. Bourasseau et al. [53] have previously considered such events by implementing the RxMC method to simulate reaction equilibria for the gas-phase, while an equation of state was used to model the condensed carbon phase. With the advancement of phase sampling techniques,

it may be possible to model both of these phases with the RxMC method. Still other applications of the RxMC method could include chemical reactions occurring within biological systems or organisms. In particular, application to protein structure prediction, such as the folding/unfolding equilibrium demonstrated by Cheung and Truskett [57], could provide a great deal of understanding in highly complex systems. These types of biological events are known to be strongly influenced by even slight changes in the surrounding environment, and the RxMC approach may be an attractive option for examining these influences.

We also reviewed several extensions and adaptations of the RxMC method, which may broaden the application of the RxMC framework to many other systems and reacting conditions in the future. Recent advances of the RxMC method have demonstrated efficient routes for modelling dense fluids and chain molecules, and future advances are anticipated which may extend the RxMC approach to other challenging cases, such as condensed-phase systems and polymer chemistry. While the RxMC method has already been shown to be useful for many applications, the quality of the results is particularly dependent upon accurate intermolecular potentials and free-energy-of-reaction data. Some of this data is already available for common systems and materials, but as novel adsorbents and chemical species are synthesised, more accurate data will be needed. Most importantly, the RxMC approach has the power to model new reactions and new reacting environments with a great deal of predictability, without the intense parameterisation often required by equation-of-state (EOS)-based calculations. Moreover, as central processing unit (CPU) speeds advance and complementary phase sampling algorithms are further developed, it is expected that RxMC can be integrated into commercial simulation packages to accurately and efficiently predict the behaviour of chemically reacting systems.

Acknowledgements

The authors wish to thank Professor Athanassios Z. Panagiotopoulos for insightful comments and Chethan Acharya for careful proofreading of the manuscript. KEG acknowledges support in part by an NSF GOALI grant no. CTS-0626031. ML acknowledges support by the Grant Agency of the Czech Republic (project No. 203/05/0725), by the Grant Agency of Academy of Sciences of the Czech Republic (project No. IAA400720710), by the National Research Programme 'Information Society' (projects No. 1ET400720507 and No. 1ET400720409), and by the Grant Programme of Academy of Sciences of the Czech Republic 'Nanotechnology for Society' (project No. KAN400720701). WRS acknowledges the support of the Natural Sciences and Research Council under Grant OGP1041, and the resources of the SHARCNET computing consortium (http://www.sharcnet.ca), which was used for some of the calculations. CHT acknoweldges financial support from DOE-EPSCoR grant no. DE-FG02-01ER45867 and computational resources from an MRAC/TeraGrid allocation.

References

[1] M. Ross, *A high-density fluid-perturbation theory based on an inverse 12th-power hard-sphere reference system*, J. Chem. Phys. 71 (1979), p. 1567.
[2] G. Zerah and J.P. Hansen, *Self-consistent integral-equations for fluid pair distribution-functions – another attempt*, J. Chem. Phys. 84 (1986), p. 2336.
[3] H.L. Vortler, I. Nezbeda, and M. Lísal, *The exp-6 potential fluid at very high pressures: computer simulations and theory*, Mol. Phys. 92 (1997), p. 813.
[4] L.E. Fried and W.M. Howard, *An accurate equation of state for the exponential-6 fluid applied to dense supercritical nitrogen*, J. Chem. Phys. 109 (1998), p. 7338.
[5] R. Dickman and G. Stell, *Self-consistent Ornstein–Zernike approximation for lattice gases*, Phys. Rev. Lett. 77 (1996), p. 996.
[6] P.T. Cummings and G. Stell, *Statistical mechanical models of chemical reactions. 1. Analytic solution of models $A + A = AB$ in the PY approximation*, Mol. Phys. 51 (1984), p. 289.
[7] ———, *Statistical mechanical models of chemical reactions. 2. Analytic solution of the Percus–Yevick approximation for a model of homogeneous association*, Mol. Phys. 55 (1985), p. 33.
[8] ———, *Statistical mechanical models of chemical reactions. 3. Solvent effects*, Mol. Phys. 60 (1987), p. 1315.
[9] W.R. Smith and R.W. Missen, *Chemical Reaction Equilibrium Analysis: Theory and Algorithms*, Wiley-Interscience, New York, 1982.
[10] E. Santiso and K.E. Gubbins, *Multi-scale molecular modeling of chemical reactivity*, Mol. Simul. 30 (2004), p. 699.
[11] D.W. Brenner, *Empirical potential for hydrocarbons for use in simulating the chemical vapor-deposition of diamond films*, Phys. Rev. E 42 (1990), p. 9458.
[12] D.W. Brenner et al., *A second-generation reactive empirical bond order (REBO) potential energy expression for hydrocarbons*, J. Phys.: Condens. Matter 14 (2002), p. 783.
[13] S.J. Stuart, A.B. Tutein, and J.A. Harrison, *A reactive potential for hydrocarbons with intermolecular interactions*, J. Chem. Phys. 112 (2000), p. 6472.
[14] ———, *Role of defects in compression and friction of anchored hydrocarbon chains on diamond*, Langmuir 16 (2000), p. 291.
[15] ———, *Indentation analysis of linear-chain hydrocarbon monolayers anchored to diamond*, J. Phys. Chem. B 103 (1999), p. 11357.
[16] P.T. Mikulski and J.A. Harrison, *Packing-density effects on the friction of* n*-alkane monolayers*, J. Am. Chem. Soc. 123 (2001), p. 6873.
[17] M.L. Elert, S.V. Zybin, and C.T. White, *Molecular dynamics study of shock-induced chemistry in small condensed-phase hydrocarbons*, J. Chem. Phys. 118 (2003), p. 9795.
[18] A.C.T. van Duin et al., *ReaxFF: a reactive force field for hydrocarbons*, J. Phys. Chem. A 105 (2001), p. 9396.
[19] P. Vashishta, R.K. Kalia, and A. Nakano, *Multimillion atom simulations of dynamics of wing cracks and nanoscale damage in glass, and hypervelocity impact damage in ceramics*, Comput. Phys. Commun. 177 (2007), p. 202.
[20] P. Vashishta et al., *Multimillion atom reactive simulations of nanostructured energetic materials*, J. Propul. Power 23 (2007), p. 688.
[21] A. Nakano et al., *A divide-and-conquer/cellular-decomposition framework for million-to-billion atom simulations of chemical reactions*, Comput. Mater. Sci. 38 (2007), p. 642.
[22] C.H. Turner et al., *Effect of confinement by porous materials on chemical reaction kinetics*, J. Chem. Phys. 116 (2002), p. 2138.

[23] J.K. Brennan, *Cavity-bias sampling in reaction ensemble Monte Carlo simulations*, Mol. Phys. 103 (2005), p. 2647.

[24] C.H. Turner, J.K. Brennan, and M. Lísal, *Replica exchange for reactive Monte Carlo simulations*, J. Phys. Chem. C 111 (2007), p. 15706.

[25] J.K. Johnson, A.Z. Panagiotopoulos, and K.E. Gubbins, *Reactive canonical Monte Carlo: a new simulation technique for reacting or associating fluids*, Mol. Phys. 81 (1994), p. 717.

[26] W.R. Smith and B. Tříska, *The reaction ensemble method for the computer simulation of chemical and phase equilibria. I. Theory and basic examples*, J. Chem. Phys. 100 (1994), p. 3019.

[27] M.S. Shaw, *Monte-Carlo simulation of equilibrium chemical-composition of molecular fluid mixtures in the* N_{atoms}PT *ensemble*, J. Chem. Phys. 94 (1991), p. 7550.

[28] ———, in *High-Pressure Science and Technology*, S.C. Schmidt et al., eds., American Institute of Physics, New York, 1994.

[29] ———, *Proceedings Tenth International Detonation Symposium*, 1994, p. 401, Office of Naval Research.

[30] ———, in *Shock Compression of Condensed Matter*, S.C. Schmidt ed., Elsevier, Amsterdam, 1992.

[31] J.K. Johnson, *Reactive canonical Monte Carlo*, in *Advances in Chemical Physics*, D.M. Ferguson, J.I. Siepmann and D.G. Truhlar, eds., Vol. 105, Wiley, New York, 1998.

[32] C.H. Turner, J.K. Johnson, and K.E. Gubbins, *Effect of confinement on chemical reaction equilibria: The reactions* $2NO \Leftrightarrow (NO)_2$ *and* $N_2 + 3H_2 \Leftrightarrow 2NH_3$, J. Chem. Phys. 114 (2001), p. 1851.

[33] J. Carrero-Mantilla and M. Llano-Restrepo, *Vapor-phase chemical equilibrium for the hydrogenation of benzene to cyclohexane from reaction-ensemble molecular simulation*, Fluid Phase Equilibr. 219 (2004), p. 181.

[34] ———, *Chemical equilibria of multiple-reaction systems from reaction ensemble Monte Carlo simulation and a predictive equation of state: combined hydrogenation of ethylene and propylene*, Fluid Phase Equilibr. 242 (2006), p. 189.

[35] L. Pusztai, H. Dominguez, and O.A. Pizio, *Reverse Monte Carlo simulation of the microscopic structure for chemically associating fluids by using experimental data*, Physica A 316 (2002), p. 65.

[36] ———, *The structure of dimerizing fluids from 'experimental' diffraction data by reverse Monte Carlo modelling*, Rev. Mex. Fis. 49 (2003), p. 212.

[37] M. Lísal, I. Nezbeda, and W.R. Smith, *The reaction ensemble method for the computer simulation of chemical and phase equilibria. II. The* $Br_2 + Cl_2 + BrCl$ *system*, J. Chem. Phys. 110 (1999), p. 8597.

[38] ———, *Molecular simulation of multicomponent reaction and phase equilibria in MTBE ternary system*, AIChE J. 46 (2000), p. 866.

[39] C.H. Turner et al. *Effect of Confinement on Chemical Reaction Equilibrium*, in *Adsorption Science and Technology*, D.D. Do ed., World Scientific, Singapore, 2001.

[40] C.H. Turner, J. Pikunic and K.E. Gubbins, *Influence of chemical and physical surface heterogeneity on chemical reaction equilibria in carbon micropores*, Mol. Phys. 99 (2001), p. 1991.

[41] C.H. Turner et al., *Simulation of chemical reaction equilibria and kinetics in heterogeneous carbon micropores*, Appl. Surf. Sci. 196 (2002), p. 366.

[42] M. Borówko et al., *Chemical reactions at surfaces: application of the reaction ensemble Monte Carlo method*, Czech. J. Phys. 48 (1998), p. 371.

[43] M. Borówko and R. Zagórski, *Chemical equilibria in slitlike pores*, J. Chem. Phys. 114 (2001), p. 5397.

[44] M. Lísal, J.K. Brennan, and W.R. Smith, *Chemical reaction equilibrium in nanoporous materials: NO dimerization reaction in carbon slit nanopores*, J. Chem. Phys. 124 (2006), p. 064712.

[45] N. Hansen, S. Jakobtorweihen, and F.J. Keil, *Reactive Monte Carlo and grand-canonical Monte Carlo simulations of the propene metathesis reaction system*, J. Chem. Phys. 122 (2005), p. 164705.

[46] ———, *Combining reactive and configurational-bias Monte Carlo: confinement influence on the propene metathesis reaction system in various zeolites*, J. Chem. Phys. 125 (2006), p. 224709.

[47] M. Lísal, W.R. Smith, and I. Nezbeda, *Computer simulation of the thermodynamic properties of high-temperature chemically-reacting plasmas*, J. Chem. Phys. 113 (2000), p. 4885.

[48] M. Lísal et al., *REMC computer simulations of the thermodynamic properties of argon and air plasmas*, Mol. Phys. 100 (2002), p. 2487.

[49] C.H. Turner and K.E. Gubbins, *Supercritical clustering and selective confinement on reaction equilibrium: a molecular simulation study of the esterification reaction*, J. Chem. Phys. 119 (2003), p. 6057.

[50] J.K. Brennan and B.M. Rice, *Molecular simulation of shocked materials using the reactive Monte Carlo method*, Phys. Rev. E 66 (2002), p. 021105.

[51] V. Bezkrovniy et al., *Reaction ensemble Monte Carlo technique and hypernetted chain approximation study of dense hydrogen*, Phys. Rev. E 69 (2004), p. 061204.

[52] V. Bezkrovniy et al., *Monte Carlo results for the hydrogen Hugoniot*, Phys. Rev. E 70 (2004), p. 057401.

[53] E. Bourasseau et al., *Molecular simulations of Hugoniots of detonation product mixtures at chemical equilibrium: microscopic calculation of the Chapman–Jouguet state*, J. Chem. Phys. 127 (2007), p. 084513.

[54] M. Lísal, W.R. Smith, and I. Nezbeda, *Accurate computer simulation of phase equilibrium for complex fluid mixtures. Application to binaries involving isobutene, methanol, methyl tert-butyl ether, and* n*-butane*, J. Phys. Chem. B 103 (1999), p. 10496.

[55] ———, *Accurate vapour–liquid equilibrium calculations for complex systems using the reaction Gibbs ensemble Monte Carlo simulation method*, Fluid Phase Equilibr. 181 (2001), p. 127.

[56] J.K. Brennan, B.M. Rice, and M. Lísal, *Simulating polymorphic phase behavior using reaction ensemble Monte Carlo*, J. Phys. Chem. C 111 (2007), p. 365.

[57] J.K. Cheung and T.M. Truskett, *Coarse-grained strategy for modeling protein stability in concentrated solutions*, Biophys. J. 89 (2005), p. 2372.

[58] W.R. Smith and M. Lísal, *Direct Monte Carlo simulation methods for nonreacting and reacting systems at fixed total internal energy or enthalpy*, Phys. Rev. E 66 (2002), p. 011104.

[59] J.K. Brennan et al., *Reaction ensemble molecular dynamics: direct simulation of the dynamic equilibrium properties of chemically reacting mixtures*, Phys. Rev. E 70 (2004), p. 061103.

[60] M. Lísal et al., *Dual control cell reaction ensemble molecular dynamics: a method for simulations of reactions and adsorption in porous materials*, J. Chem. Phys. 121 (2004), p. 4901.

[61] ———, *Mesoscale simulation of polymer reaction equilibrium: combining dissipative particle dynamics with reaction ensemble Monte Carlo. I. Polydispersed polymer systems*, J. Chem. Phys. 125 (2006), p. 164905.

[62] D.A. McQuarrie, *Statistical Mechanics*, Harper Collins, New York, 1976.

[63] J.S. Rowlinson, *The perfect gas*, *International Encyclopedia of Physical Chemistry and Chemical Physics*, Topic 10, Vol. 5, McMillan Co., New York, 1963.

[64] J.B. Pedley, *Thermodynamical Data and Structures of Organic Compounds*, *TRC Data Series*, Thermodynamic Research Center, College Station, TX, 1994.

[65] M.W. Chase, Jr., *NIST-JANAF Thermochemical Tables*, 4th ed., Journal of Physical and Chemical Reference Data, Monograph 9 American Physical Society, Melville, NY, 1988.

[66] D. Frenkel and B. Smit, *Understanding Molecular Simulation*, Academic Press, San Diego, 2002.

[67] A.Z. Panagiotopoulos, *Direct determination of phase coexistence properties of fluids by Monte Carlo simulation in a new ensemble*, Mol. Phys. 61 (1987), p. 813.

[68] A.Z. Panagiotopoulos et al., *Phase-equilibria by simulation in the Gibbs ensemble – alternative derivation, generalization*

and application to mixture and membrane equilibria, Mol. Phys. 63 (1988), p. 527.
[69] L.F. Rull, G. Jackson, and B. Smit, *The condition of microscopic reversibility in Gibbs ensemble Monte Carlo simulations of phase equilibria*, Mol. Phys. 85 (1995), p. 435.
[70] J.L. deGarmo, V.N. Parulekar, and V. Pinjala, *Consider reactive distillation*, Chem. Eng. Prog. 88 (1992), p. 43.
[71] D.F. Coker and R.O. Watts, *Computer simulation of reactive liquids in chemical equilibrium*, Chem. Phys. Lett. 78 (1981), p. 333.
[72] ———, *Chemical equilibria in mixtures of bromine and chlorine*, Mol. Phys. 44 (1981), p. 1303.
[73] D.A. Kofke and E.D. Glandt, *Monte Carlo simulation of multicomponent equilibria in a semigrand ensemble*, Mol. Phys. 64 (1988), p. 1105.
[74] W.L. Jorgensen, J.D. Madura, and C.J. Swensen, *Optimized intermolecular potential functions for liquid hydrocarbons*, J. Am. Chem. Soc. 106 (1984), p. 6638.
[75] W.L. Jorgensen, *Optimized intermolecular potential functions for liquid alcohols*, J. Phys. Chem. 90 (1986), p. 1276.
[76] J.M. Briggs, T. Matsui, and W.L. Jorgensen, *Monte-Carlo simulations of liquid alkyl ethers with the OPLS potential functions*, J. Comput. Chem. 11 (1990), p. 958.
[77] B.R. Brooks et al., *CHARMM: A program for macromolecular energy, minimization, and dynamics calculations*, J. Comput. Chem. 4 (1983), p. 187.
[78] L.E. Fried, *Cheetah 3.0 User's Manual*, manuscript number UCRL-MA-117541 [Revision 3] Lawrence Livermore National Laboratory, Livermore, 2001.
[79] F.H. Ree, *A statistical mechanical theory of chemically reacting multiphase mixtures: application to the detonation properties of PETN*, J. Chem. Phys. 81 (1984), p. 1251.
[80] S.C. McGrother and K.E. Gubbins, *Constant pressure Gibbs ensemble Monte Carlo simulations of adsorption into narrow pores*, Mol. Phys. 97 (1999), p. 955.
[81] S. Tripathi and W. G. Chapman, *A density functional approach to chemical reaction equilibria in confined systems: application to dimerization*, J. Chem. Phys. 118 (2003), p. 7993.
[82] J. Pikunic et al., *Improved molecular models for porous carbons*, Stud. Surf. Sci. Catal. 132 (2001), p. 647.
[83] C. Baerlocher, W.M. Meier, and D.H. Olson, *Atlas of Zeolite Framework Types*, Elsevier Science, Amsterdam, 2001.
[84] J.M. van de Graaf et al., *Application of a zeolite membrane reactor in the metathesis of propene*, Chem. Eng. Sci. 54 (1999), p. 1441.
[85] ———, *Application of a silicalite-1 membrane reactor in metathesis reactions*, Appl. Catal. A: Gen. 178 (1999), p. 225.
[86] K.A. Dill, *Theory for the folding and stability of globular-proteins*, Biochemistry-US 24 (1985), p. 1501.
[87] K.A. Dill, D.O.V. Alonso, and K. Hutchinson, *Thermal stabilities of globular-proteins*, Biochemistry-US 28 (1989), p. 5439.
[88] V.K. Shen et al., *Coarse-grained strategy for modeling protein stability in concentrated solutions. II: phase behavior*, Biophys. J. 90 (2006), p. 1949.
[89] J.K. Cheung et al., *Coarse-grained strategy for modeling protein stability in concentrated solutions. III: directional protein interactions*, Biophys. J. 92 (2007), p. 4316.
[90] I. Benjamin, *Chemical reaction dynamics at liquid interfaces: a computational approach*, Prog. React. Kin. Mech. 27 (2002), p. 87.
[91] C.H. Turner, *Monte Carlo simulation of equilibrium reactions at vapor–liquid interfaces*, J. Phys. Chem. B 109 (2005), p. 23588.
[92] ———, *Monte Carlo simulation of equilibrium reactions at modified vapor–liquid interfaces*, Langmuir 23 (2007), p. 2525.
[93] J.H. Seinfeld and S.N. Pandis, *Atmospheric Chemistry and Physics*, Wiley, New York, 1998.
[94] H. Eyring, *The theory of absolute reaction rates*, Trans. Faraday Soc. 34 (1938), p. 41.
[95] W.F.K. Wynne-Jones and H. Eyring, *The absolute rate of reactions in condensed phases*, J. Chem. Phys. 3 (1935), p. 492.
[96] H. Eyring, *The activated complex in chemical reactions*, J. Chem. Phys. 3 (1935), p. 107.
[97] M.G. Evans and M. Polanyi, *Some applications of the transition state method to the calculation of reaction velocities, especially in solution*, Trans. Faraday Soc. 31 (1935), p. 875.
[98] H.W. Graben and J.R. Ray, *Eight physical systems of thermodynamics, statistical-mechanics, and computer-simulations*, Mol. Phys. 80 (1993), p. 1183.
[99] T. Kristóf and J. Liszi, *Alternative implementations of the Gibbs ensemble Monte Carlo calculation*, Chem. Phys. Lett. 261 (1996), p. 620.
[100] M. Lísal, W.R. Smith, and K. Aim, *Direct molecular-level Monte Carlo simulation of Joule–Thomson processes*, Mol. Phys. 101 (2003), p. 2875.
[101] M. Lísal, M. Bendová, and W.R. Smith, *Monte Carlo adiabatic simulation of equilibrium reacting systems: the ammonia synthesis reaction*, Fluid Phase Equilibr. 235 (2005), p. 50.
[102] J.M.D. MacElroy, *Nonequilibrium molecular-dynamics simulation of diffusion and flow in thin microporous membranes*, J. Chem. Phys. 101 (1994), p. 5274.
[103] G.S. Heffelfinger and F. van Swol, *Diffusion in Lennard-Jones fluids using dual control-volume grand-canonical molecular-dynamics simulation (DCV-GCMD)*, J. Chem. Phys. 100 (1994), p. 7548.
[104] W.R. Smith and M. Lísal, *Molecular simulation of reaction and adsorption in nanochemical devices: increase of reaction conversion by separation of a product from the reactant mixture*, in *ICCSA 2004, LNCS 2004*, A. Lagana, et al., eds., Springer-Verlag, Berlin, 2004.
[105] M. Mezei, *A cavity-biased (T, V, μ) Monte Carlo method for the computer simulation of fluids*, Mol. Phys. 40 (1980), p. 901.
[106] B. Smit, *Grand-canonical Monte-Carlo simulations of chain molecules – adsorption-isotherms of alkanes in zeolites*, Mol. Phys. 85 (1995), p. 153.
[107] G.C.A.M. Mooij, D. Frenkel, and B. Smit, *Direct simulation of phase-equilibria of chain molecules*, J. Phys.: Condens. Matter 4 (1992), p. L255.
[108] J.K. Brennan, M. Lísal, and C.H. Turner, *Reaction ensemble Monte Carlo simulation of the Hugoniot curve for nitromethane*, (in preparation) (2008)
[109] R. H. Swendsen and J. S. Wang, *Replica Monte-Carlo simulation of spin-glasses*, Phys. Rev. Lett. 57 (1986), p. 2607.
[110] K. Hukushima, and K. Nemoto, *Exchange Monte Carlo method and application to spin glass simulations*, J. Phys. Soc. Jpn. 65 (1996), p. 1604.
[111] J.P. Neirotti et al., *Phase changes in 38-atom Lennard-Jones clusters. I. A parallel tempering study in the canonical ensemble*, J. Chem. Phys. 112 (2000), p. 10340.
[112] U.H.E. Hansmann, *Parallel tempering algorithm for conformational studies of biological molecules*, Chem. Phys. Lett. 281 (1997), p. 140.
[113] J. Czwartos et al., *Freezing and melting of azeotropic mixtures confined in nanopores: experiment and molecular simulation*, Mol. Phys. 103 (2005), p. 3103.
[114] Q. Yan and J.J. de Pablo, *Hyperparallel tempering Monte Carlo simulation of polymeric systems*, J. Chem. Phys. 113 (2000), p. 1276.
[115] F. Calvo et al., *Phase changes in 38-atom Lennard-Jones clusters. II. A parallel tempering study of equilibrium and dynamic properties in the molecular dynamics and microcanonical ensembles*, J. Chem. Phys. 112 (2000), p. 10350.
[116] H. Fukunishi, O. Watanabe, and S. Takada, *On the Hamiltonian replica exchange method for efficient sampling of biomolecular systems: application to protein structure prediction*, J. Chem. Phys. 116 (2002), p. 9058.
[117] Y. Sugita, A. Kitao, and Y. Okamoto, *Multidimensional replica-exchange method for free-energy calculations*, J. Chem. Phys. 113 (2000), p. 6042.
[118] P.J. Hoogerbrugge and J.M.V.A. Koelman, *Simulating microscopic hydrodynamic phenomena with dissipative particle dynamics*, Europhys. Lett. 19 (1992), p. 155.
[119] J.M.V.A. Koelman and P.J. Hoogerbrugge, *Dynamic simulations of hard-sphere suspensions under steady shear*, Europhys. Lett. 21 (1993), p. 363.

[120] Y. Kong et al., *Simulation of a confined polymer in solution using the dissipative particle dynamics method*, Int. J. Thermophys. 15 (1994), p. 1093.
[121] A.G. Schlijper, P.J. Hoogerbrugge, and C.W. Manke, *Computer-simulation of dilute polymer-solutions with the dissipative particle dynamics method*, J. Rheol. 39 (1995), p. 567.
[122] M. Lísal, J.K. Brennan, and W.R. Smith, *Mesoscale simulation of polymer reaction equilibrium: combining dissipative particle dynamics with reaction ensemble Monte Carlo. II. Supramolecular diblock copolymer systems*, (in preparation) (2008).
[123] M.P. Allen and D.J. Tildesley, *Computer Simulation of Liquids*, Clarendon Press, Oxford, 1987.
[124] M. Lísal, W.R. Smith, and J. Kolafa, *Molecular simulations of aqueous electrolyte solubility: 1. The expanded-ensemble osmotic molecular dynamics method for the solution phase*, 109 (2005), p. 12956.
[125] W.J. Nellis et al., *Equation-of-state, shock-temperature, and electrical-conductivity data of dense fluid nitrogen in the region of the dissociative phase-transition*, J. Chem. Phys. 94 (1991), p. 2244.
[126] V.N. Zubarev and G.S. Telegin, *The impact compressibility of liquid nitrogen and solid carbon dioxide*, Sov. Phys. Dokl. 7 (1962), p. 34.
[127] B. Militzer and D.M. Ceperley, *Path integral Monte Carlo calculation of the deuterium Hugoniot*, Phys. Rev. Lett. 85 (2000), p. 1890.
[128] S.A. Bonev, B. Militzer, and G. Galli, Ab initio *simulations of dense liquid deuterium: comparison with gas-gun shock-wave experiments*, Phys. Rev. B 69 (2004), p. 014101.
[129] F. Charlet et al., *Evaluation of various theoretical equations of state used in calculation of detonation properties*, J. Appl. Phys. 84 (1998), p. 4227.